Supplemental Information

Engineering Heteroatomic Structures in Pt Single-Atom Anchored Covalent Organic Frameworks for Enhanced Photocatalytic Hydrogen Evolution Reaction

Wenqi Tang[a], Jianrong Zeng[c], Fenggang Bian[c], Huiming Lin*[b], Huanyu Zhao*[a], Zhong-Yuan Lu*[a]

[a] Institute of Theoretical Chemistry, College of Chemistry, Jilin University, Changchun 130023, China
[b] Laboratory for Photon and Electronic Bandgap Materials, College of Chemistry and Chemical Engineering, Harbin Normal University, Harbin 150025, China
[c] Shanghai Synchrotron Radiation Facility, Shanghai Advanced Research Institute, Chinese Academy of Sciences, 201204 Shanghai, P. R. China

E-mail: linhuiming@hrbnu.edu.cn, zhaohuanyu@jlu.edu.cn, luzhy@jlu.edu.cn

1. Characterizations

^{1}H NMR spectra were recorded on the Bruker-Avance III 400MHz spectrometer. Fourier transform infrared (FTIR) spectra were recorded on a Bruker VERTEX 80V spectrometer. Thermogravimetric analysis (TGA) was carried out under nitrogen atmosphere on a NETZSCH STA449F3 QMS403D analyzer. Powder X-ray diffraction (XRD) data were collected on Rigaku Smartlab diffractometer using a Cu Kα source (λ = 1.5418 Å) over the range of 2θ = 3.0−35.0 with a step size of 0.02° and 2 s per step. The sorption isotherm for N_2 was measured by using a Micromeritics ASAP 2020 PlusHD88 analyzer. The SEM images were obtained on Regulus 8100 microscope. The TEM images were obtained on JEM-2100 Electron Microscope. The AC HAADF-STEM images were obtained on JEM-ARM300F. X-ray photoelectron spectroscopy (XPS) patterns were measured on ESCALAB 250. Ultraviolet photo-electron spectroscopy (UPS) patterns were measured on Thermo Fisher ESCALAB 250XI (He I α). The actual amount of Pt was determined by inductively coupled plasma optical emission spectroscopy (ICP-OES) on iCAP. The solid-state UV-Vis diffuse reflection spectrum (UV-Vis-DRS) were obtained on Lambda 950 spectrometer using $BaSO_4$ as a reference. The photoluminescence (PL) spectra and PL decay profiles were measured on FL1000 spectrometer with the excitation wavelength at 400 nm. The contact number (CA) was measured on Theta Flex. XAFS spectra were performed on the beamline BL13SSW in SSRF (Shanghai).

2. Performances evaluations:

Electrochemical characterizations:

Mott-Schottky plots, EIS plots and I−t profiles were measured on the CHI 760 electrochemical station in a standard three electrode configuration. The working electrode was prepared by the following method: 2.5 mg powder was added into a solution of 100 μL ethanol and 10 μL 5 wt% Nafion solution. Then the mixture was ultrasonicated over 30 min to get a suspension, 10 μL of the suspension was further drop-casted onto Indium-tin oxide (ITO) glass (1 × 1 cm^2) and dried in an oven at 70 ℃. Employed a platinum plate electrode as the counter electrode, a saturated Ag/AgCl electrode as the reference electrode, and a 0.1 M Na_2SO_4 solution was used as the electrolyte.

Apparent quantum yields:

The apparent quantum yields (AQY) of catalysts were measured using band-pass filters under different wavelengths (420 nm, 450 nm, 500 nm and 600 nm). The AQY was calculated using the following equation:

$$\text{AQY (\%)} = \frac{Ne}{Np} = \frac{10^9 \left(\nu\, N_A\, K\right)\left(h\, c\right)}{\left(I\, A\, \lambda\right)}$$

Ne is the total number of electrons transferred by the reaction; Np is incident photon number; ν is the reaction rate (mol s^{-1}); N_A is the Avogadro's number; K is the number of electrons transferred by the reaction; h is the Planck constant; c is the velocity of light (m s^{-1}); I is the incident light area (W m^{-2}); A is the incident light area (m^{-2}); λ is the incident wavelength (nm).

XAS data analysis:

XAS data were processed and analyzed using the Demeter software package[1]. The Fourier transformed fitting was carried out under the k^3 weighting, the k-range of 3−12 Å^{-1}, and R range of 1−3 Å were utilized for fittings. The four parameters—coordination number, bond length, Debye−Waller factor, and E_0 shift (N, R, σ^2, and ΔE_0) —were fitted without any being fixed, constrained, or correlated. For Wavelet Transform analysis, the $\chi(k)$ exported from Athena was imported into the Hama Fortran code. The parameters were listed as follow: k range, 0−12 Å^{-1}; k weight, 2; R range, 1−4 Å; and Morlet function with $\kappa = 10$, $\sigma = 1$ was employed.

3. Computational details

Structural modelling. Structural modeling of COFs was constructed using Materials Studio (version 2020) suite of programs. Geometry optimization was conducted with MS DMol3 module. The calculated powder X-ray diffraction (PXRD) patterns were generated with the Reflex module.

Density functional theory calculations. DFT calculations of charge distribution and adsorption energy were performed in the Vienna Ab-initio Simulation Package (VASP). The projector-augmented wave (PAW) method was used to describe the electron–ion interaction. The generalized gradient approximation expressed by Perdew-Burke-Ernzerh (PBE) of functional and a plane-wave cutoff energy of 500 eV were used in all computations. The electronic structure calculations were employed with a Gaussian smearing of 0.05 eV for all calculations. The Monkhorst mesh of 3 × 3 × 1 k-point was chosen to sample the Brillouin zone. The convergence of energy and forces were set to 1 ×10^{-5} eV and 0.05 eV Å^{-1}, respectively.

In each calculation task, the 1 × 1 one-layer model of the COF was employed and all the atoms were fully relaxed in geometric optimizing, and the slabs have a 20.0 Å vacuum layer.

The free energy diagrams for the H_2 evolution reaction were calculated, in which the chemical potential of a proton/ electron ($H^+ + e^-$) is equal to half of that of one H_2 gas molecule. The change in free energy (ΔG_{H^*}) in the overall transformation was determined according to Eq. (1)[2].

$$\Delta G_{H^*} = E_{H^*+cat.} - E_{cat.} - \frac{1}{2} E_{H2} + \Delta E_{ZPE} - T\Delta S \quad (1)$$

where $E_{H^*+cat.}$, $E_{cat.}$, E_{H2}, ΔE_{ZPE}, and ΔS represent the total energy for adsorption H, the energy of the bare catalyst, the energy of gaseous H_2, the zero-point energy change, and the entropy change between H^+ and H_2, respectively.

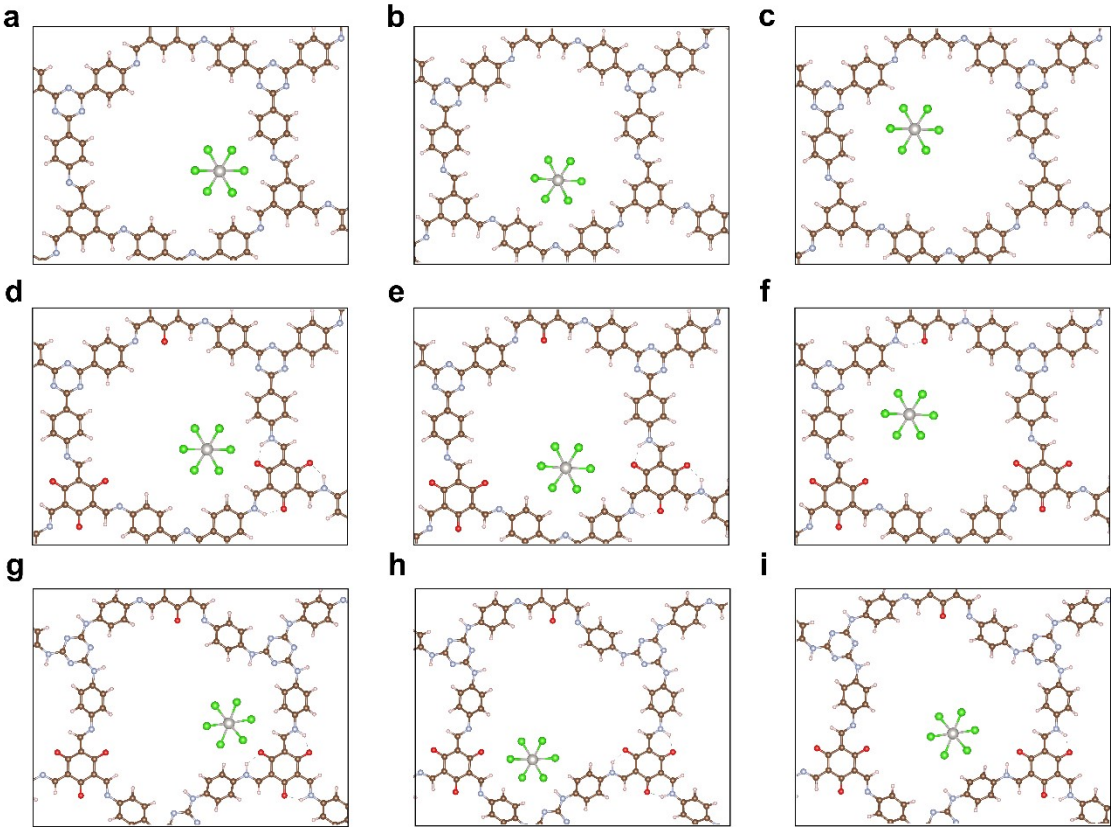

Figure S1. Optimized configurations of $PtCl_6^{2-}$ adsorbing on COFs, a-c, site 1-3 of TAPA-TFB. d-f, site 1-3 of TAPA-TFP. g-i, site 1-3 of TAPAT-TFP.

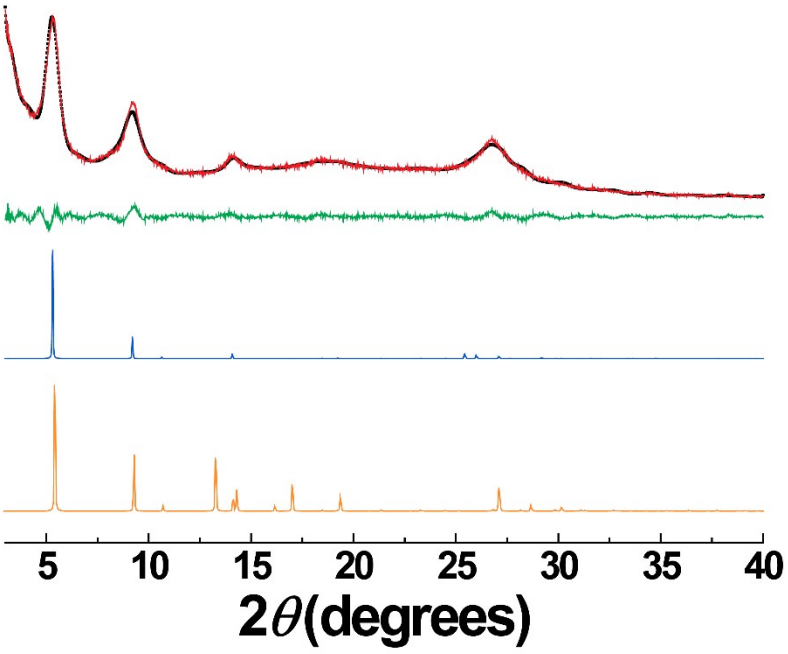

Figure S2. Pawley refined XRD curves of TAPAT-TFP (red: refined data, black: experimental data, green: difference, blue: simulated data of AA structure, orange: simulated data of AB structure).

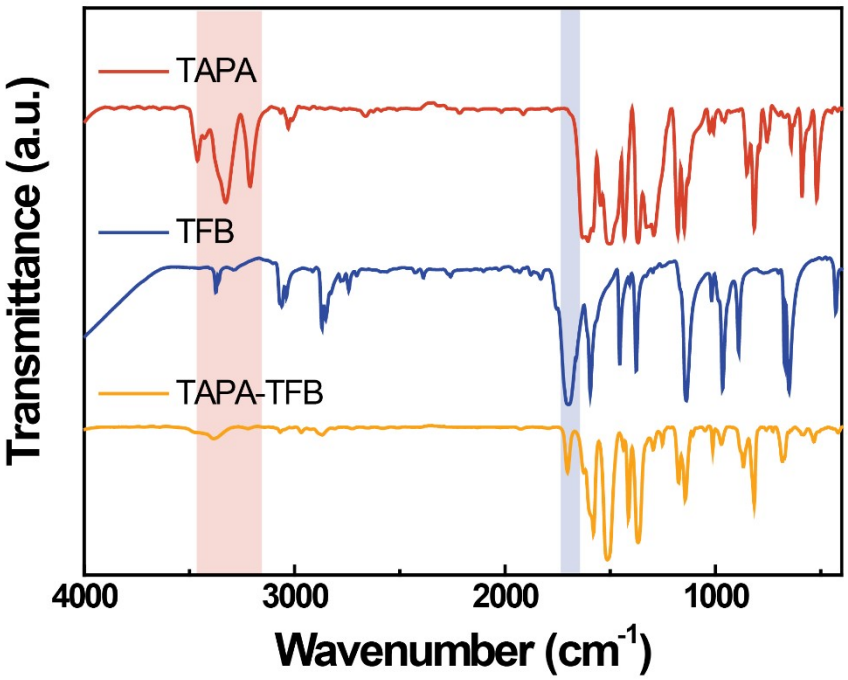

Figure S3. FT-IR spectra of TAPA, TFB and TAPA-TFB.

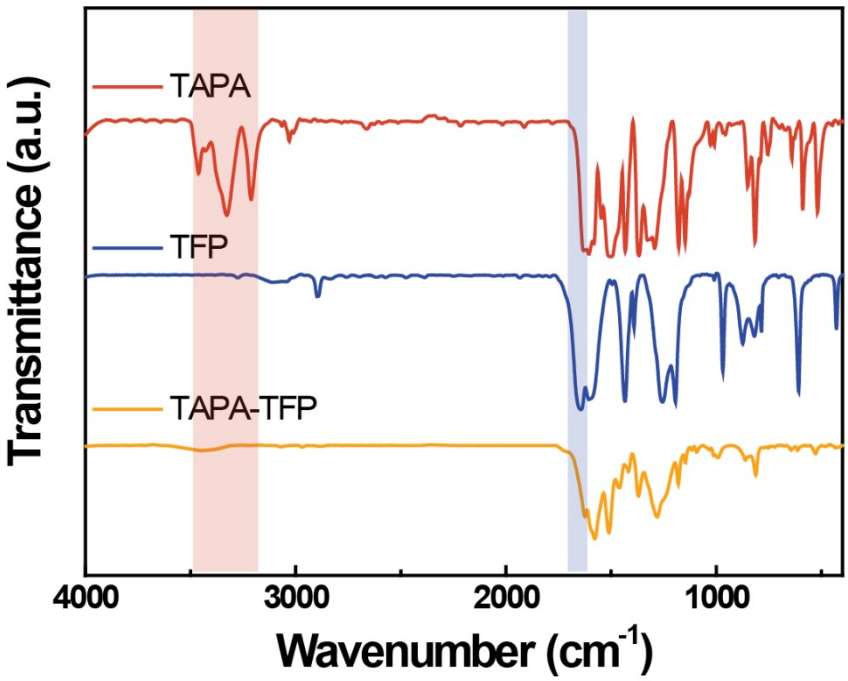

Figure S4. FT-IR spectra of TAPA, TFP and TAPA-TFP.

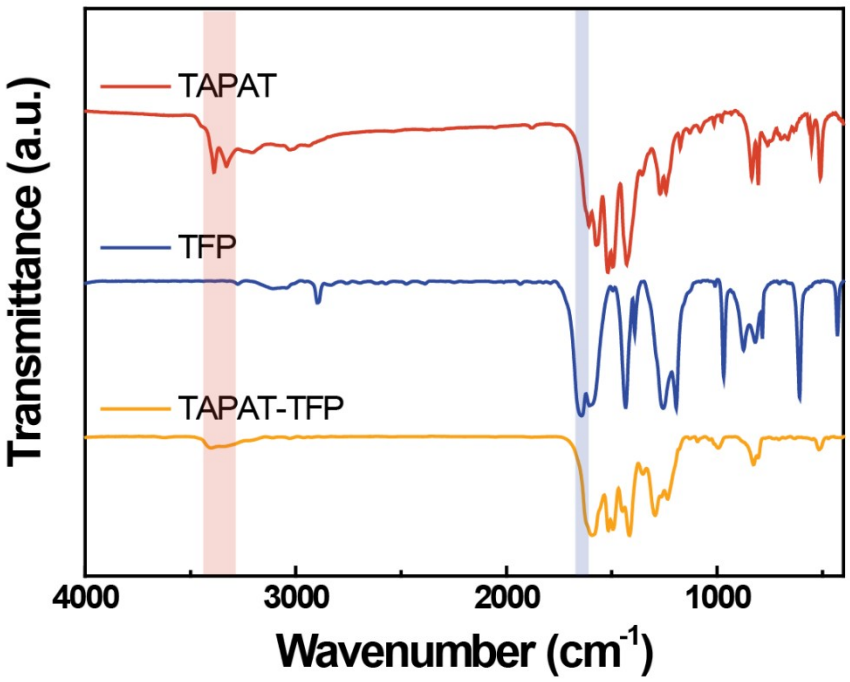

Figure S5. FT-IR spectra of TAPAT, TFP and TAPAT-TFP.

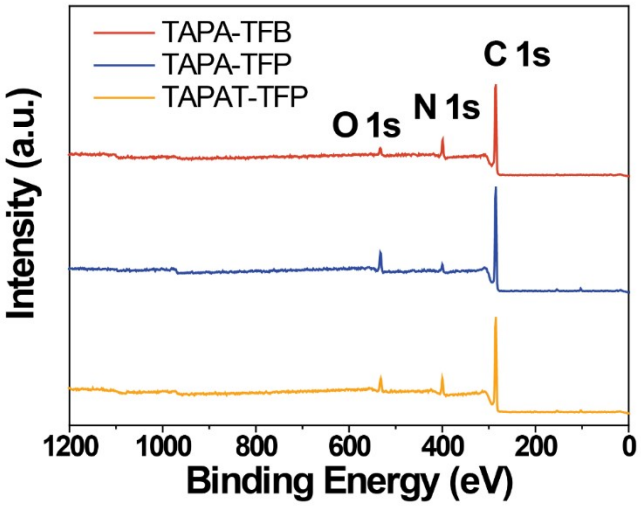

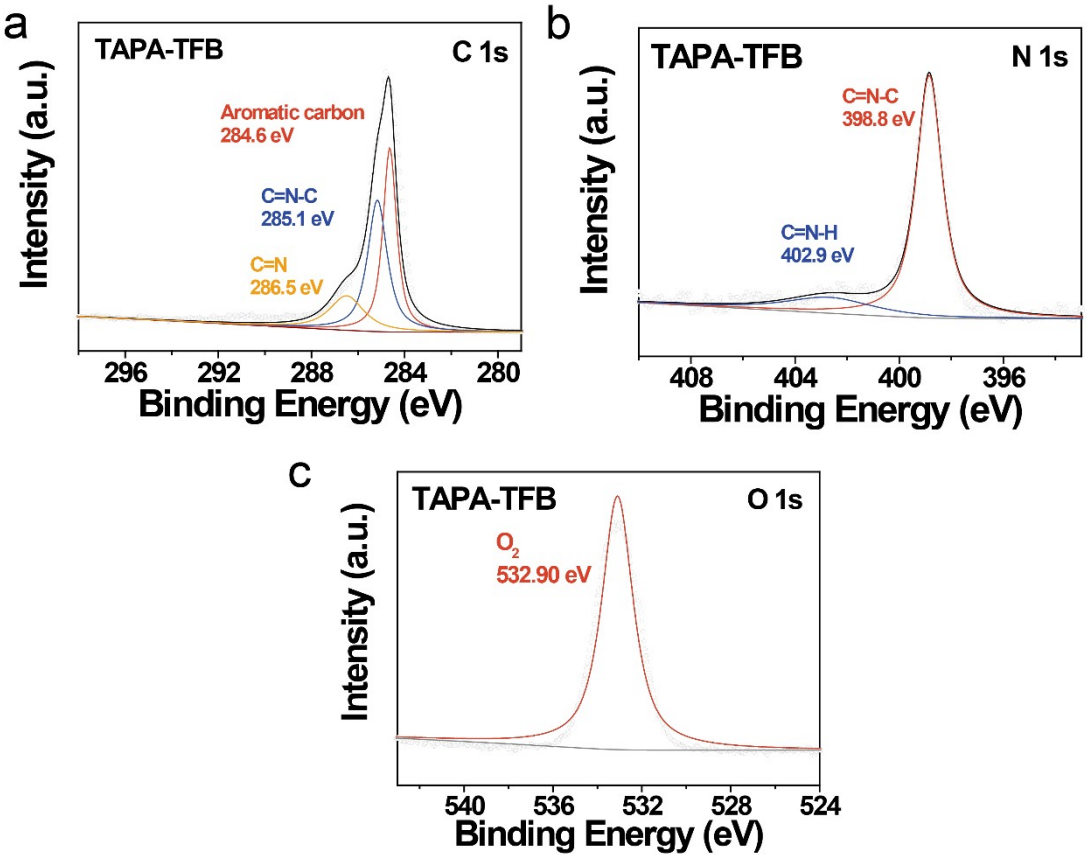

Figure S6. XPS survey spectra.

Figure S7. a, C 1s, b, N 1s and c, O 1s high-resolution XPS spectra of TAPA-TFB.

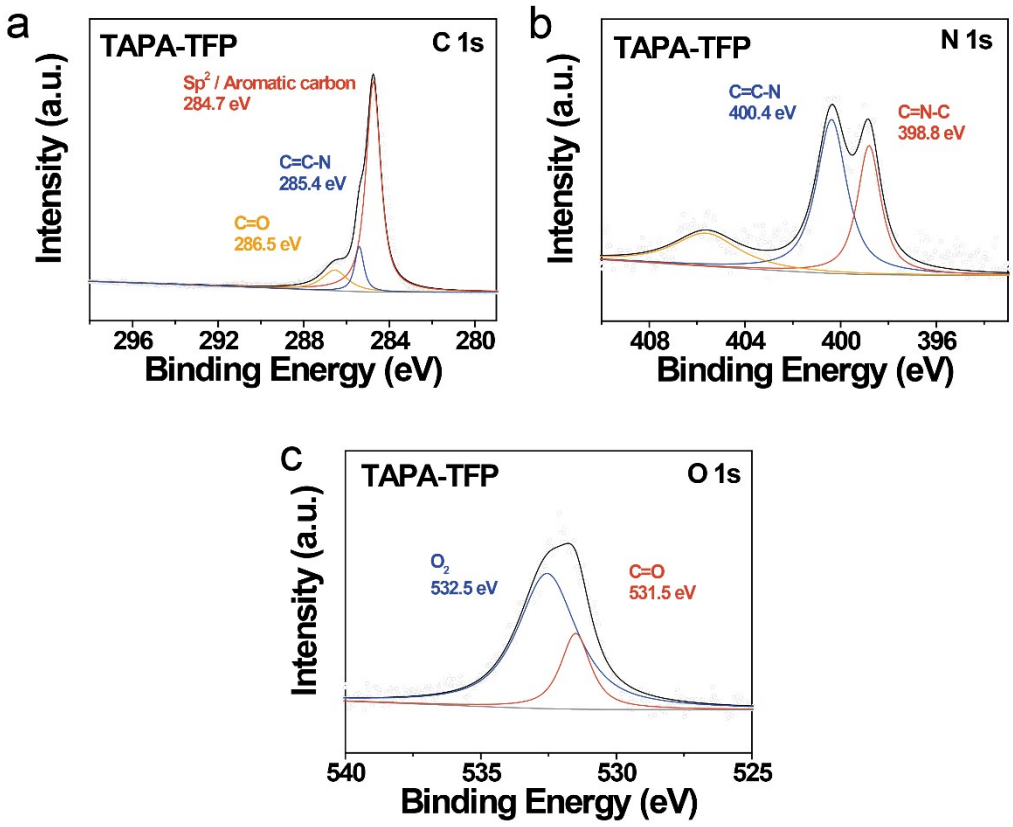

Figure S8. a, C 1s, b, N 1s and c, O 1s high-resolution XPS spectra of TAPA-TFP.

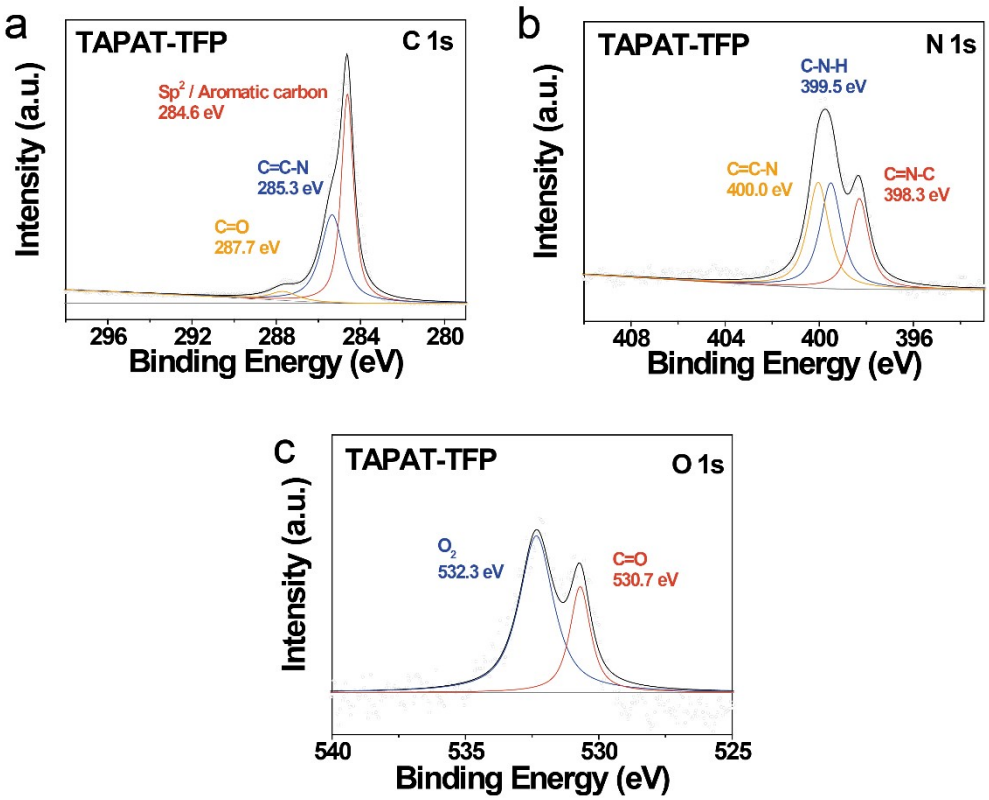

Figure S9. a, C 1s, b, N 1s and c, O 1s high-resolution XPS spectra of TAPAT-TFP.

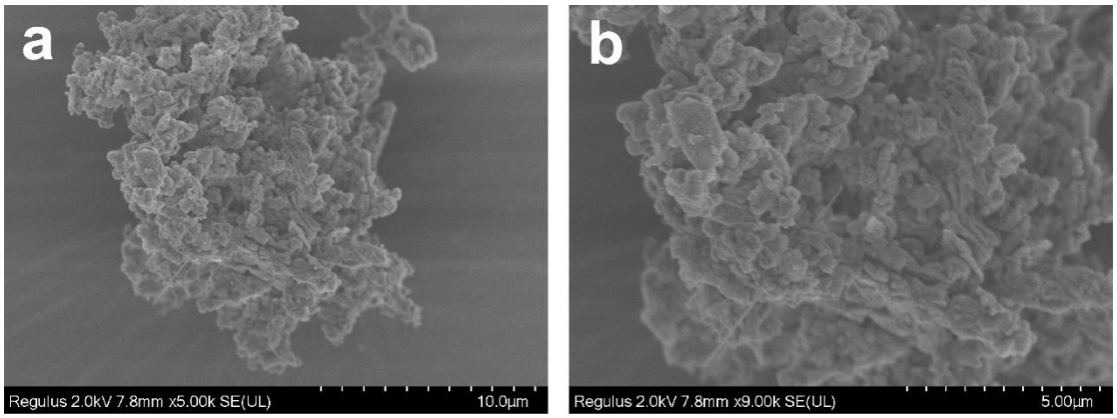

Figure S10. SEM images of TAPA-TFB.

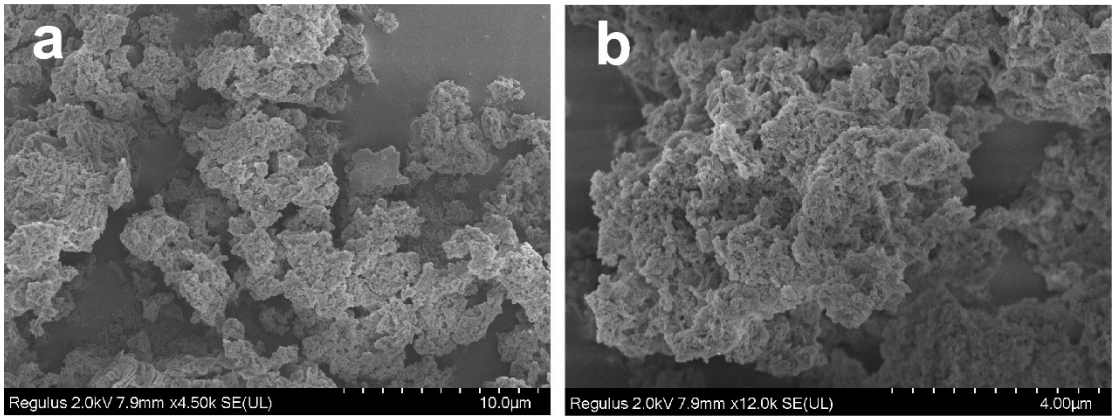

Figure S11. SEM images of TAPA-TFP.

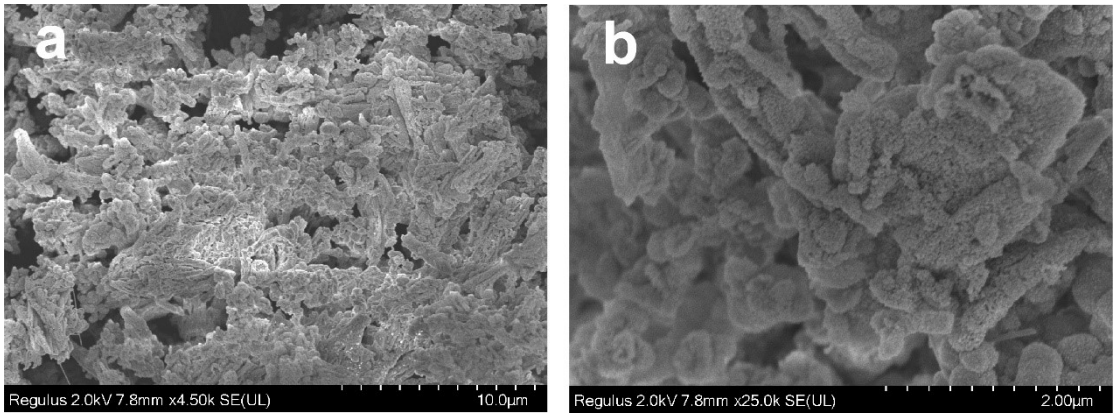

Figure S12. SEM images of TAPAT-TFP.

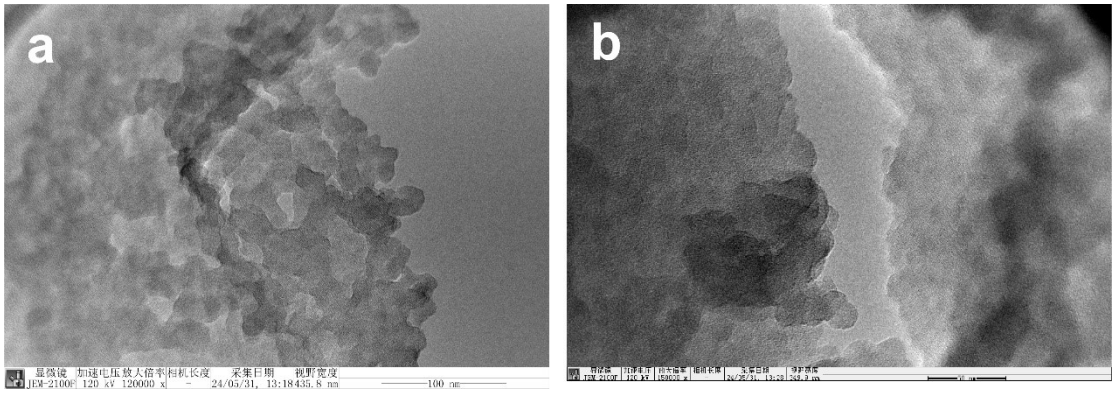

Figure S13. TEM images of TAPA-TFB.

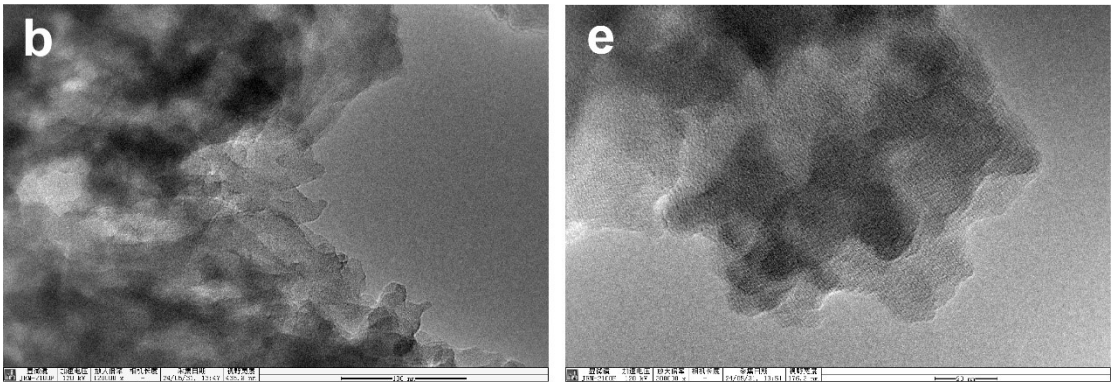

Figure S14. TEM images of TAPA-TFP.

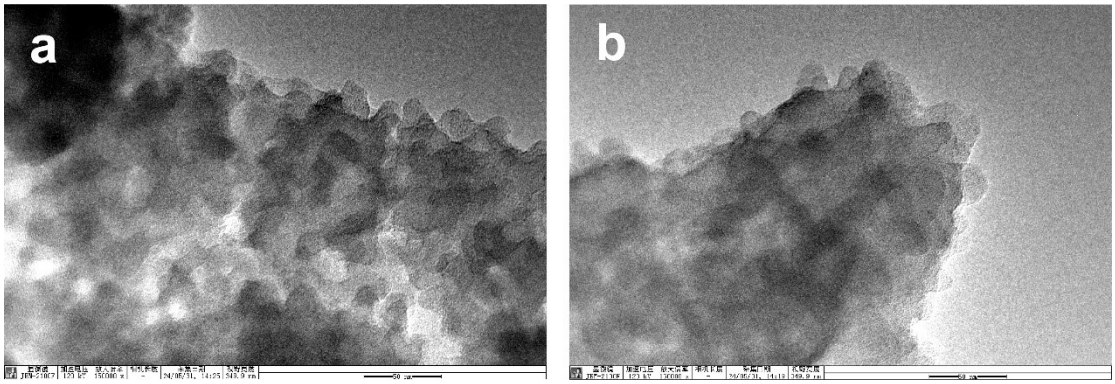

Figure S15. TEM images of TAPAT-TFP.

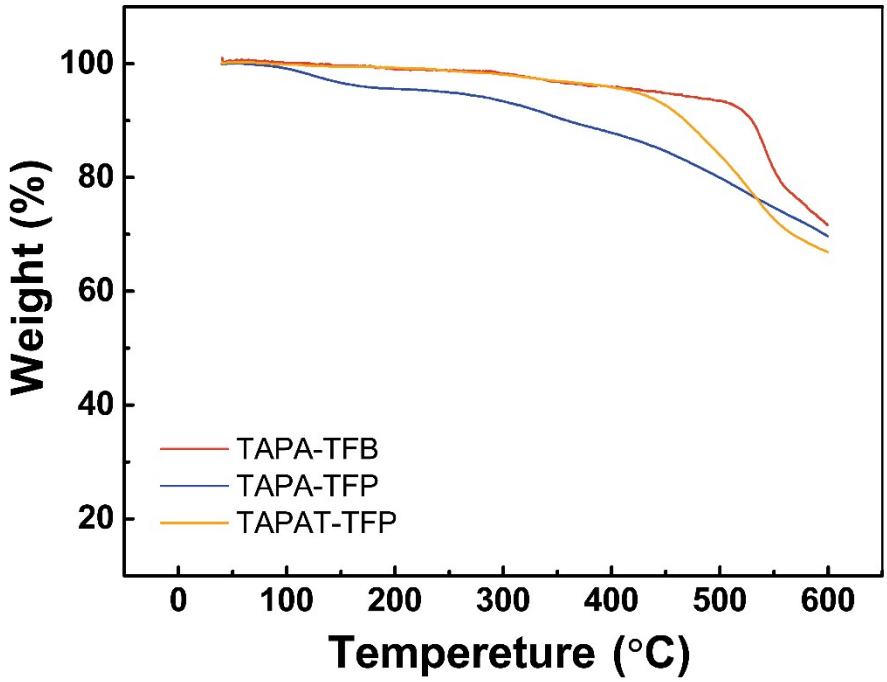

Figure S16. TGA curves of TAPA-TFB (red), TAPA-TFP (blue) and TAPAT-TFP (orange)

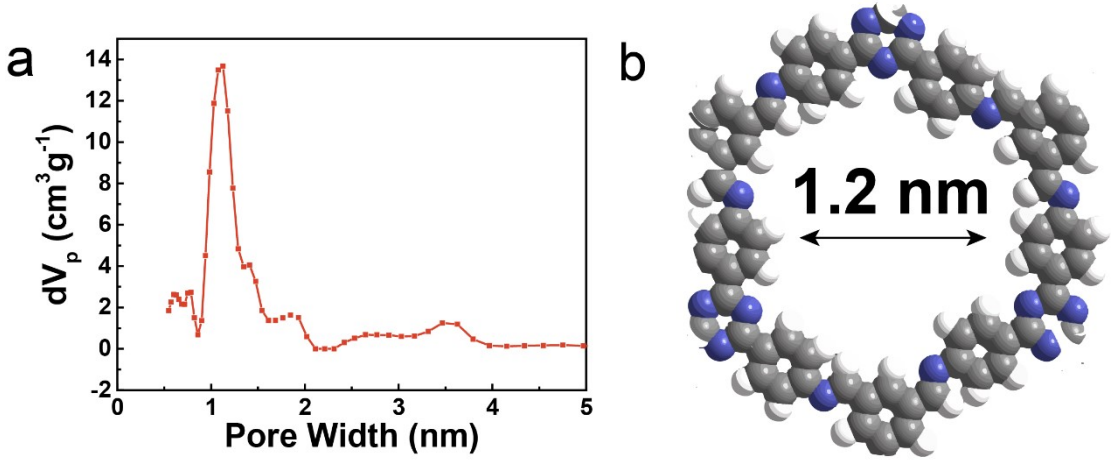

Figure S17. a, pore size distribution of TAPA-TFB. b, calculated pore size diameter of TAPA-TFB.

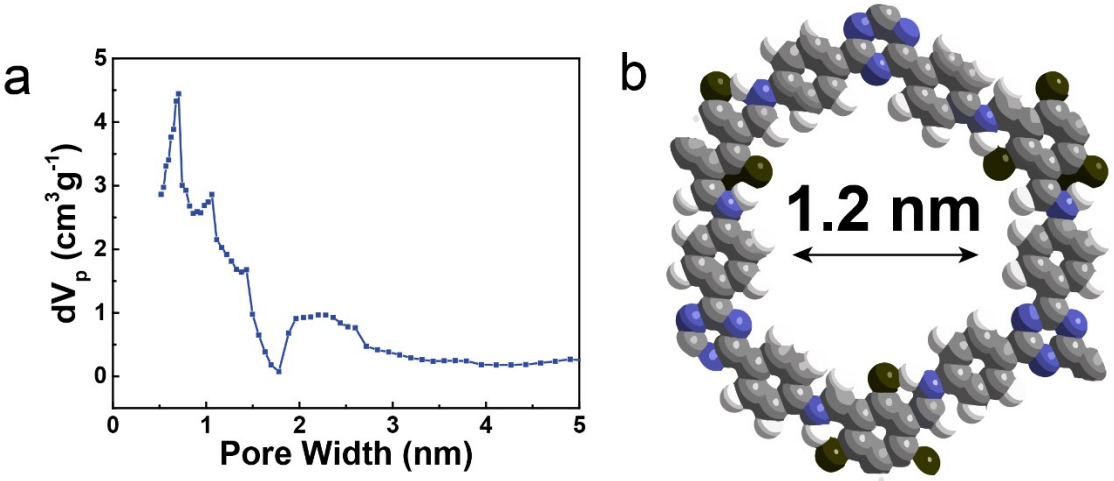

Figure S18. a, pore size distribution of TAPA-TFP. b, calculated pore size diameter of TAPA-TFP.

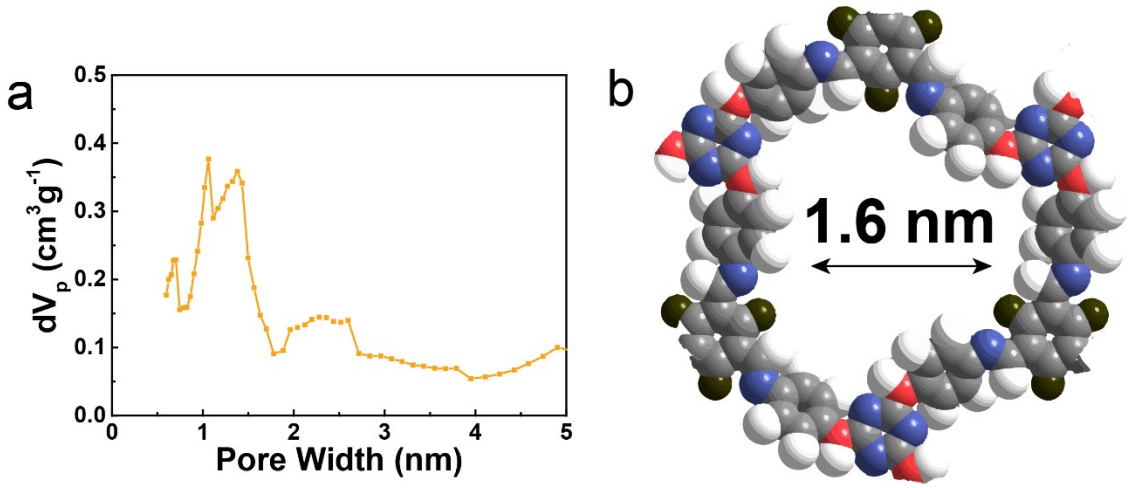

Figure S19. a, pore size distribution of TAPAT-TFP. b, calculated pore size diameter of TAPAT-TFP.

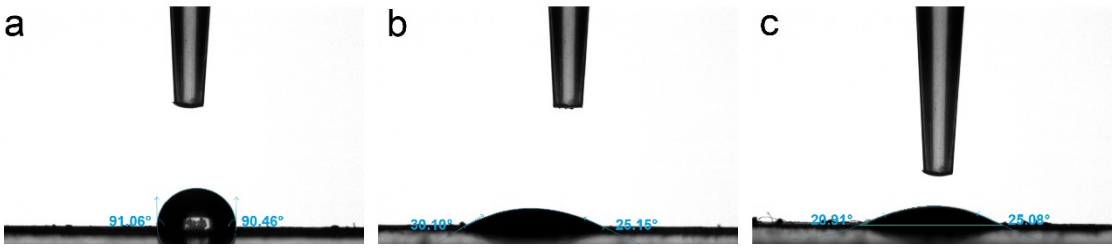

Figure S20. Static water contact angle measurements of a, TAPA-TFB; b, TAPA-TFP; c, TAPAT-TFP.

Figure S21. Photographs of TAPA-TFB (a), TAPA-TFP (b) and TAPAT-TFP (c).

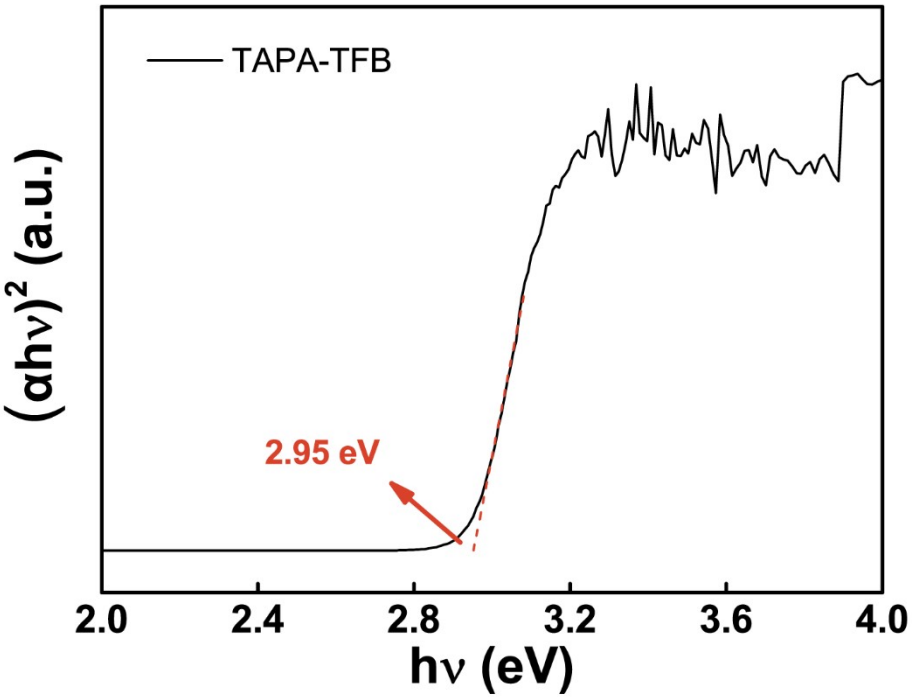

Figure S22. Tauc plot of TAPA-TFB.

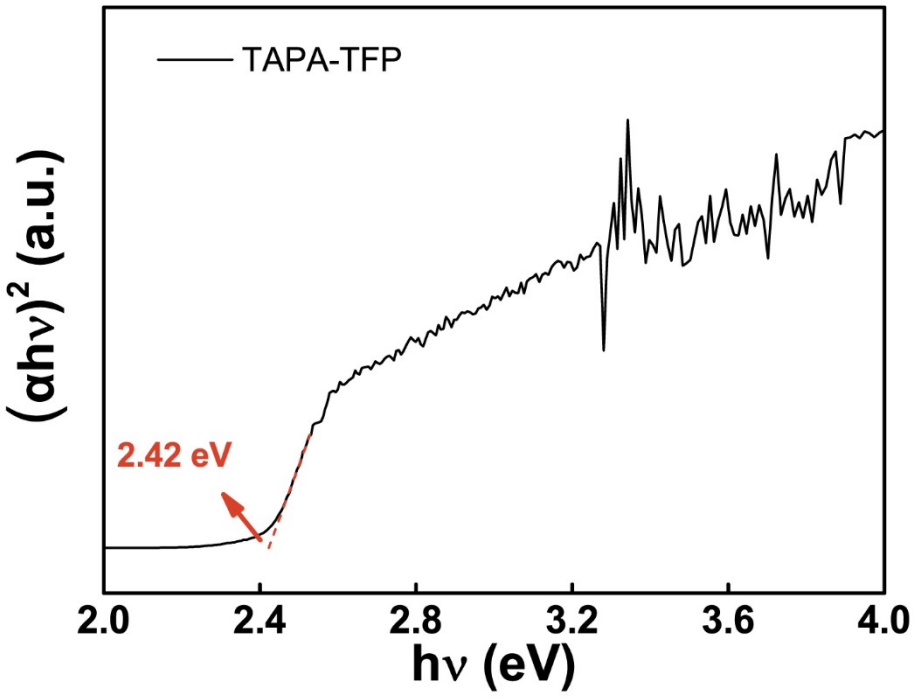

Figure S23. Tauc plot of TAPA-TFP.

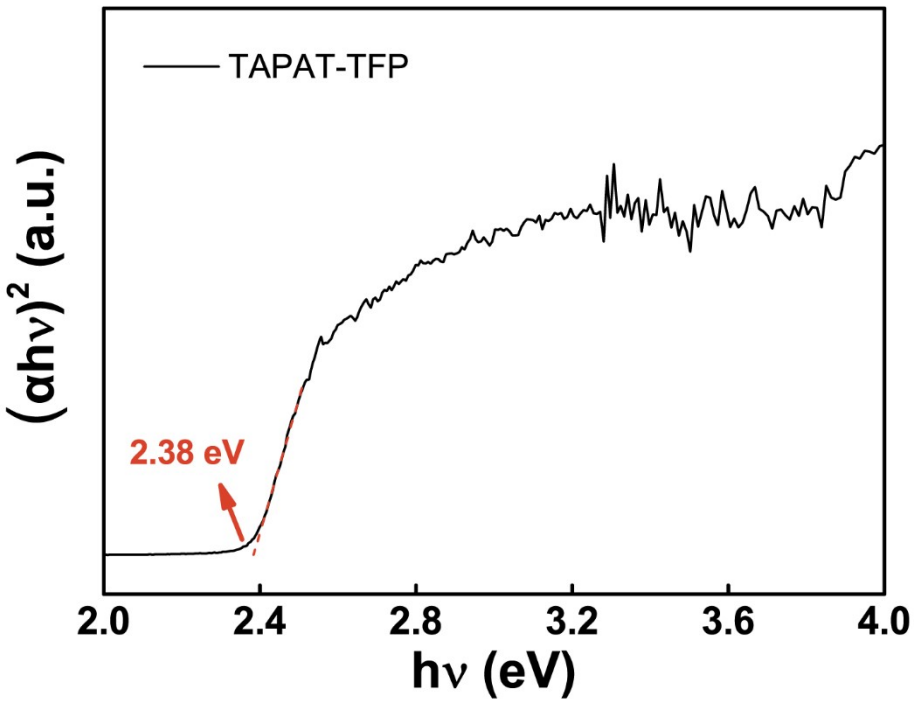

Figure S24. Tauc plot of TAPAT-TFP.

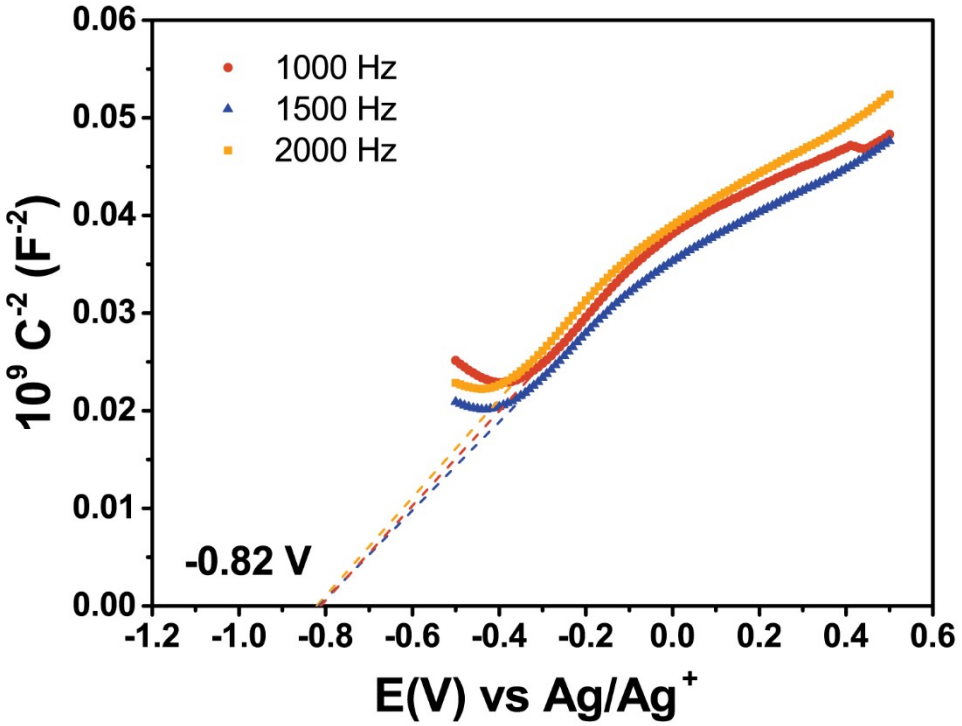

Figure S25. Mott-Schottky (M-S) plots of TAPA-TFB.

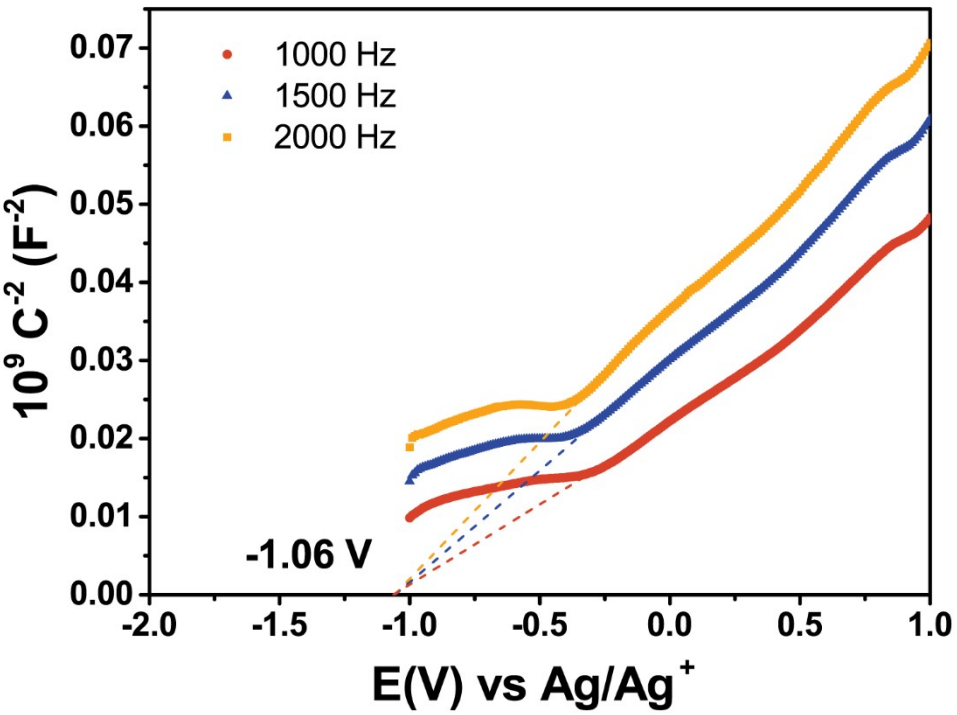

Figure S26. Mott-Schottky (M-S) plots of TAPA-TFP.

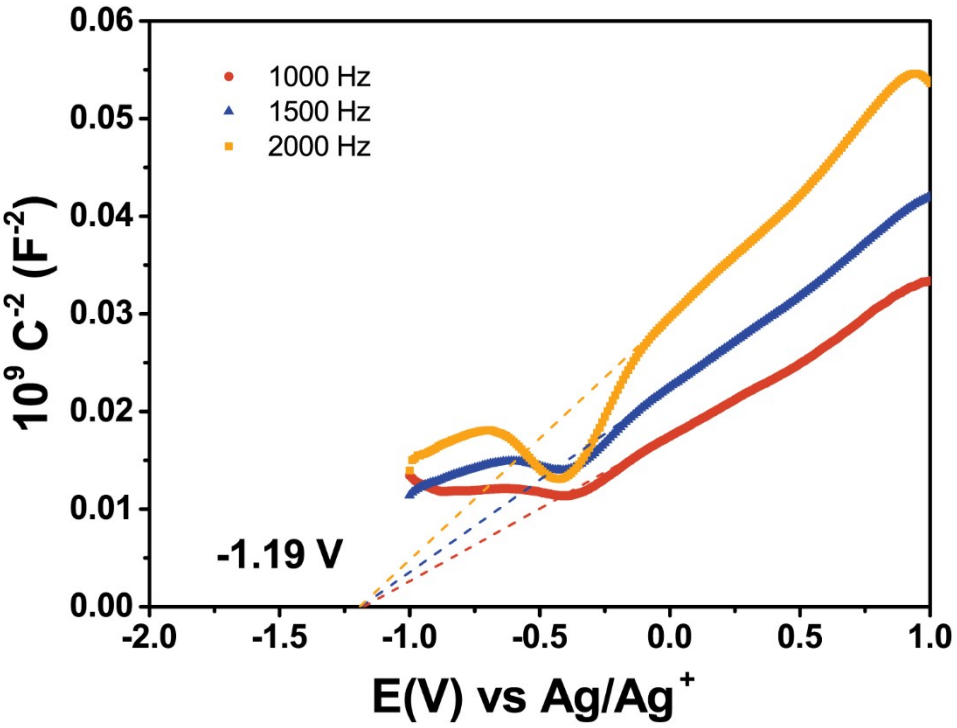

Figure S27. Mott-Schottky (M-S) plots TAPAT-TFP.

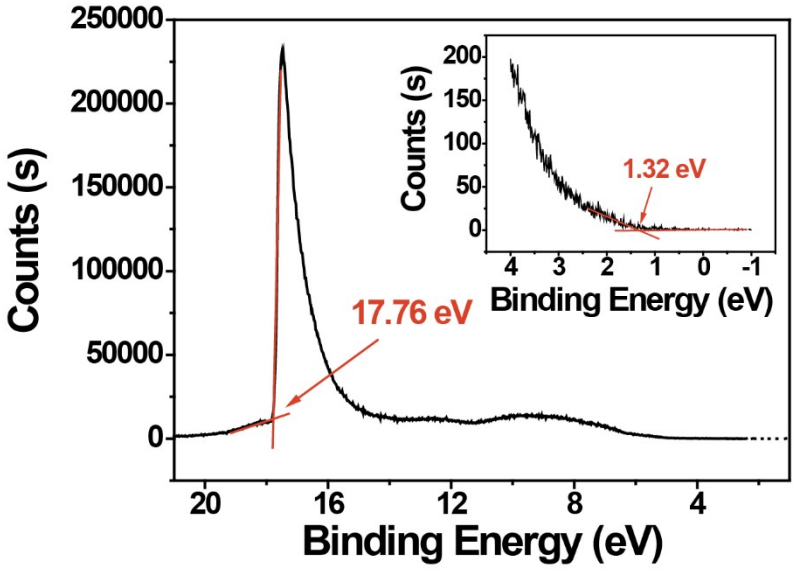

Figure S28. Ultraviolet Photoelectron Spectroscopy (UPS) spectrum of TAPA-TFB.

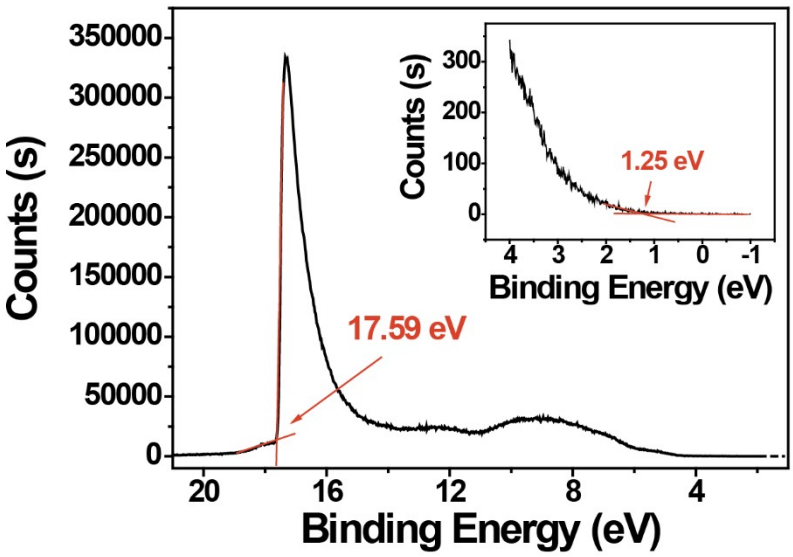

Figure S29. UPS spectrum of TAPA-TFP.

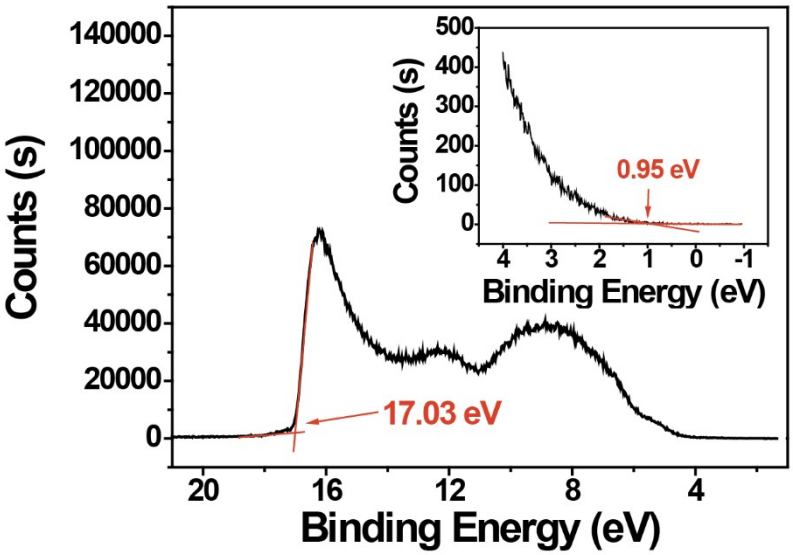

Figure S30. UPS spectrum of TAPAT-TFP.

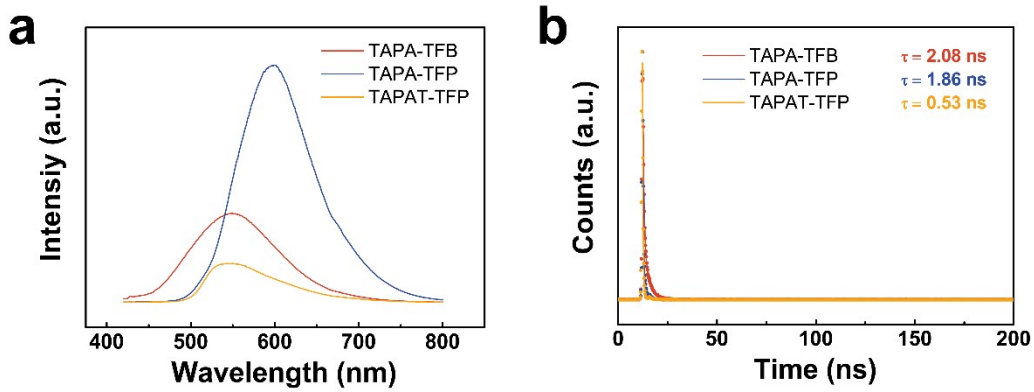

Figure S31. a, photoluminescence (PL) spectra of TAPA-TFB, TAPA-TFP and TAPAT-TFP (excitation wavelength: 400 nm). b, PL decay plots.

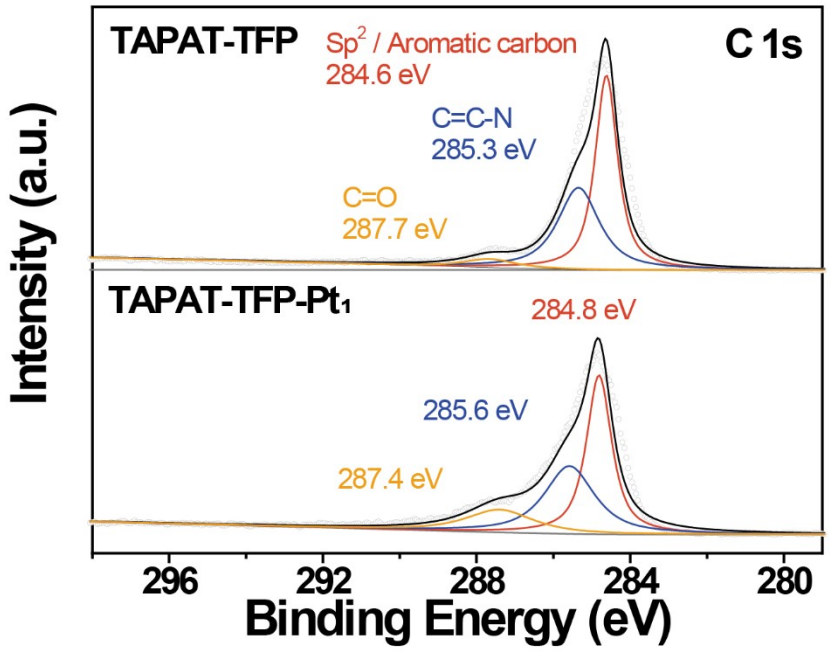

Figure S32. The high-resolution C 1s XPS spectra of pristine TAPAT-TFP and TAPAT-TFP-Pt_1.

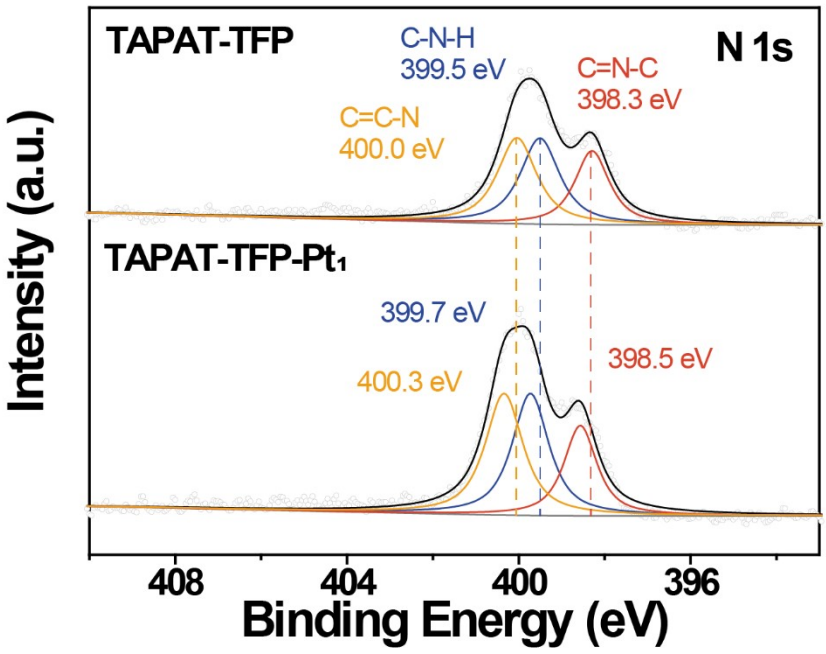

Figure S33. The high-resolution N 1s XPS spectra of pristine TAPAT-TFP and TAPAT-TFP-Pt_1.

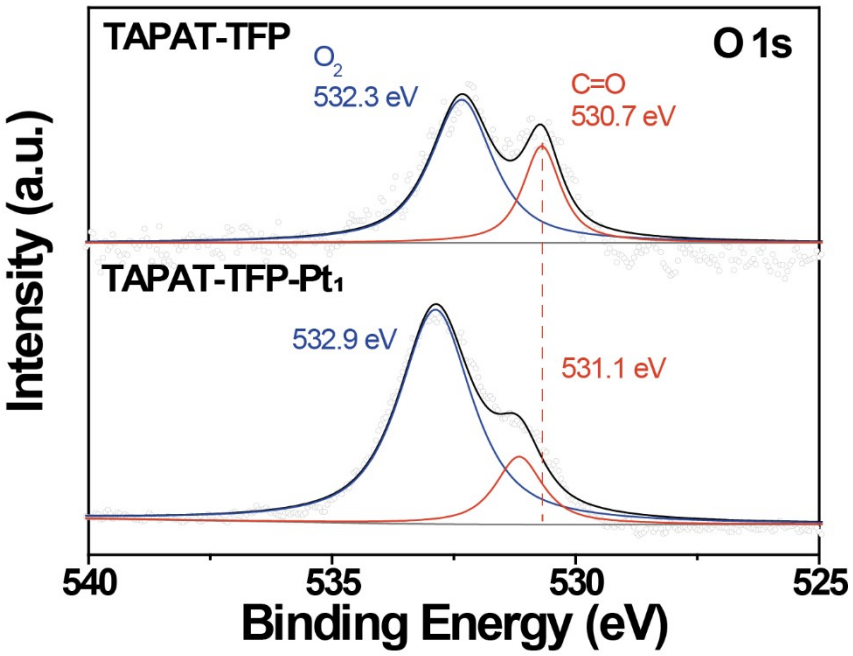

Figure S34. The high-resolution O 1s XPS spectra of pristine TAPAT-TFP and TAPAT-TFP-Pt_1.

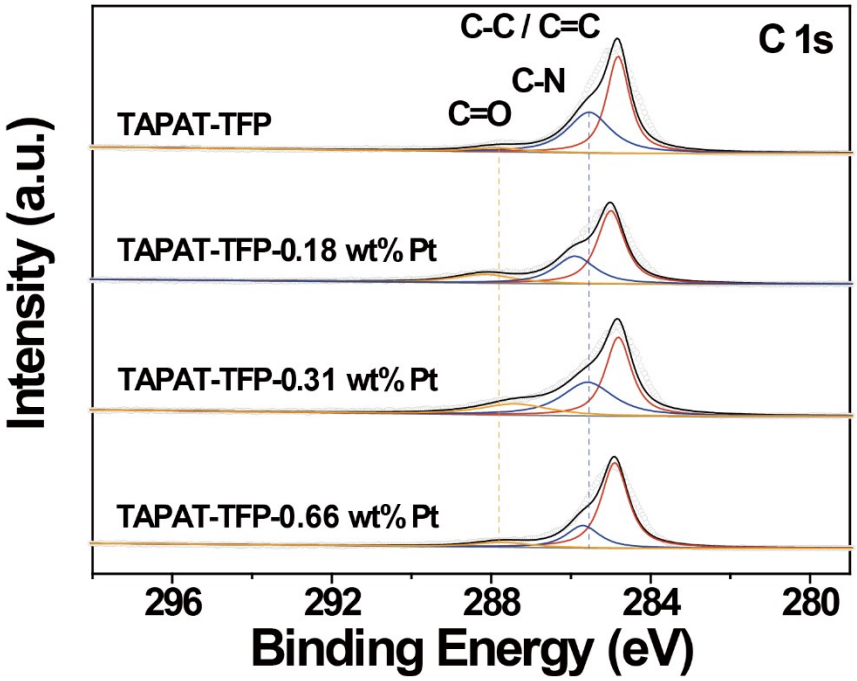

Figure S35. The high-resolution C 1s XPS spectra of pristine TAPAT-TFP, TAPAT-TFP-Pt_1-0.18 wt% Pt, TAPAT-TFP-Pt_1-0.31 wt% Pt and TAPAT-TFP-Pt_1-0.66 wt% Pt.

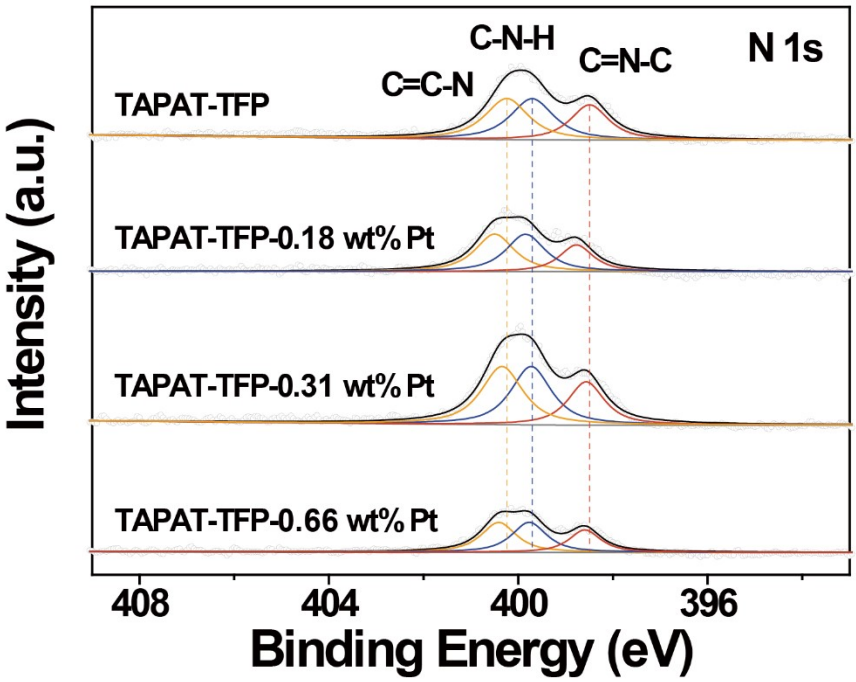

Figure S36. The high-resolution N 1s XPS spectra of pristine TAPAT-TFP, TAPAT-TFP-Pt_1-0.18 wt% Pt, TAPAT-TFP-Pt_1-0.31 wt% Pt and TAPAT-TFP-Pt_1-0.66 wt% Pt.

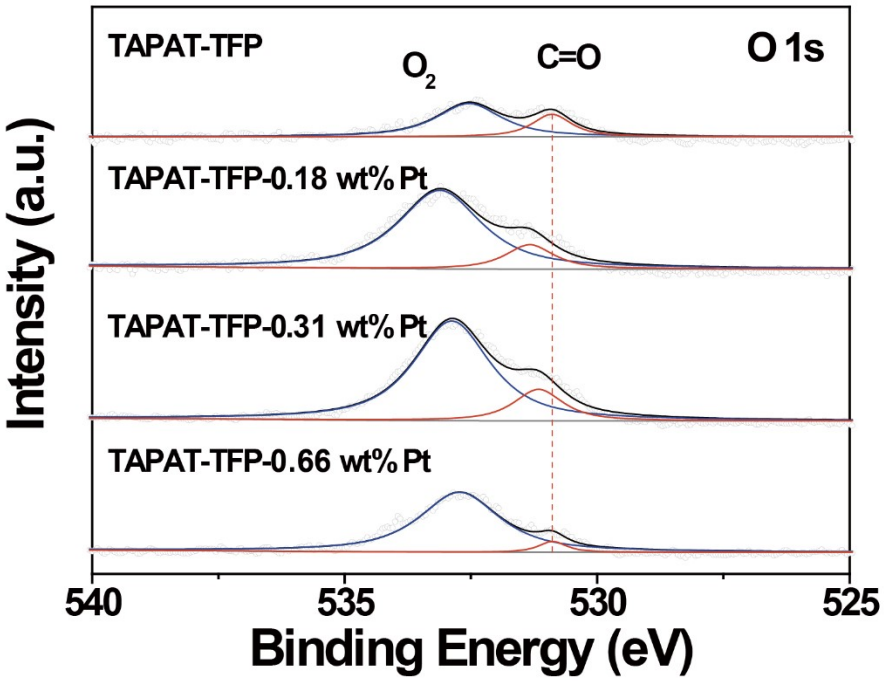

Figure S37. The high-resolution O 1s XPS spectra of pristine TAPAT-TFP, TAPAT-TFP-Pt_1-0.18 wt% Pt, TAPAT-TFP-Pt_1-0.31 wt% Pt and TAPAT-TFP-Pt_1-0.66 wt% Pt.

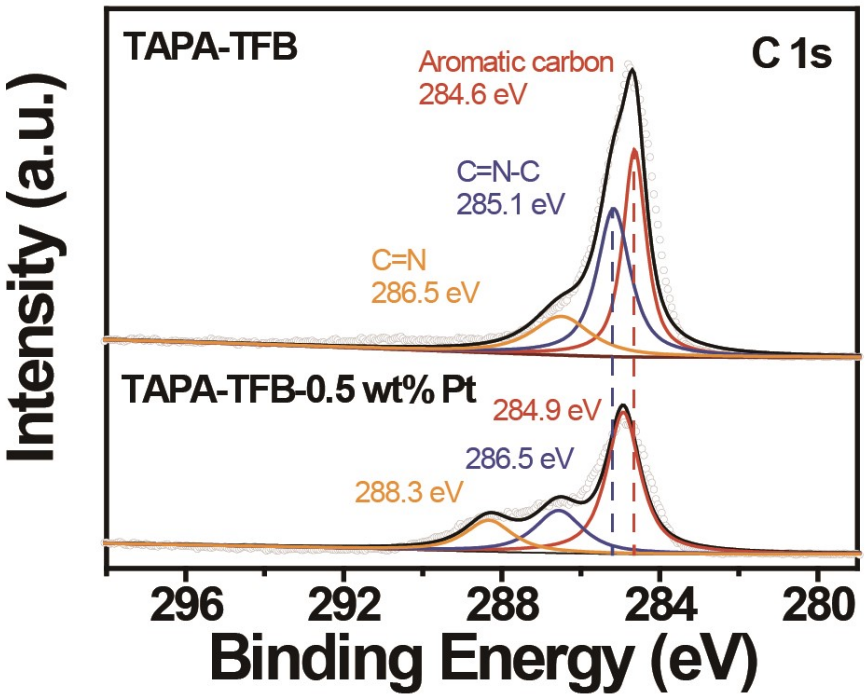

Figure S38. The high-resolution C 1s XPS spectra of pristine TAPA-TFB and COF with Pt additive amount of 0.5 wt%.

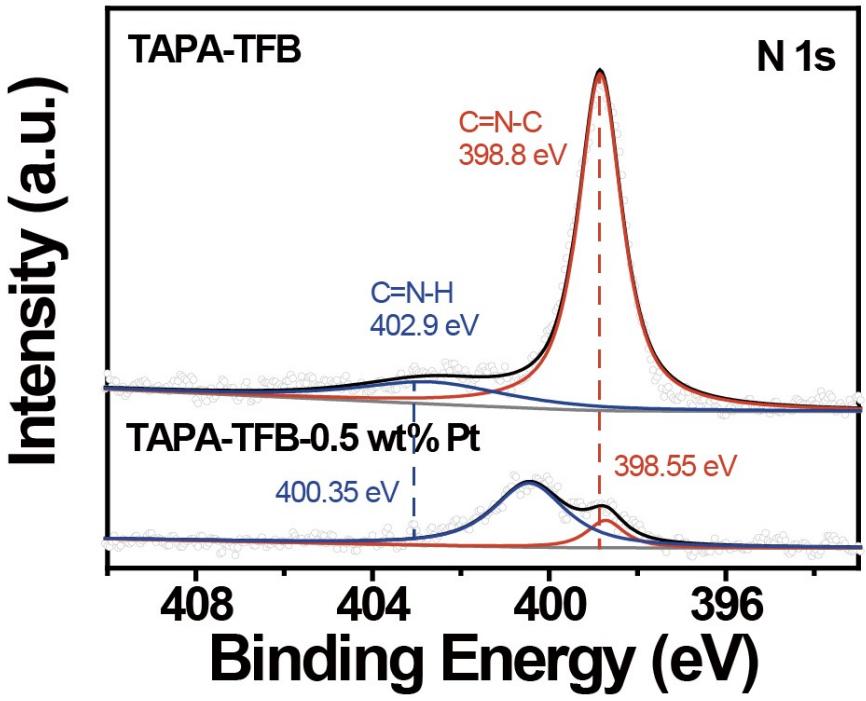

Figure S39. The high-resolution N 1s XPS spectra of pristine TAPA-TFB and COF with Pt additive amount of 0.5 wt%.

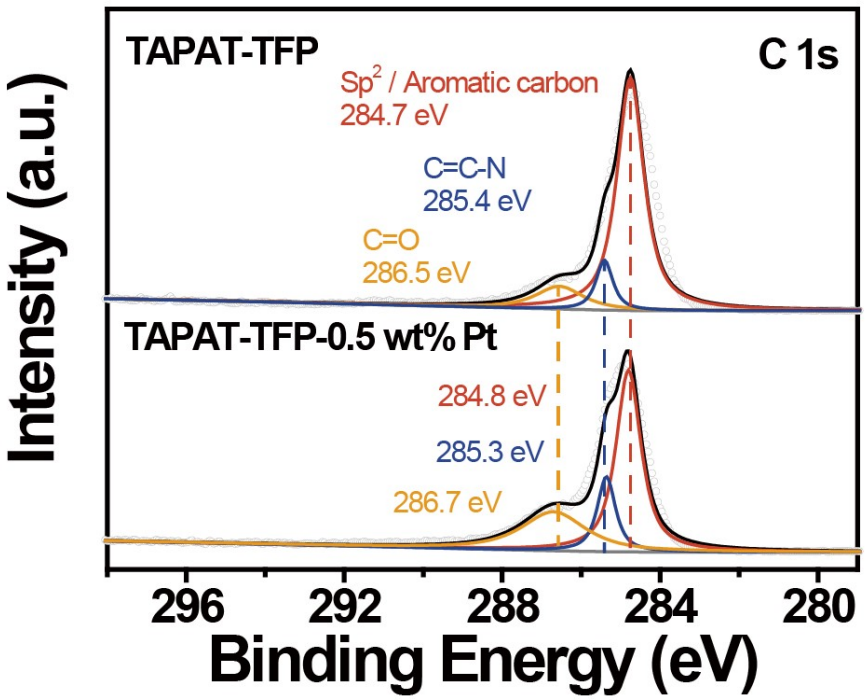

Figure S40. The high-resolution C 1s XPS spectra of pristine TAPA-TFP and COF with Pt additive amount of 0.5 wt%.

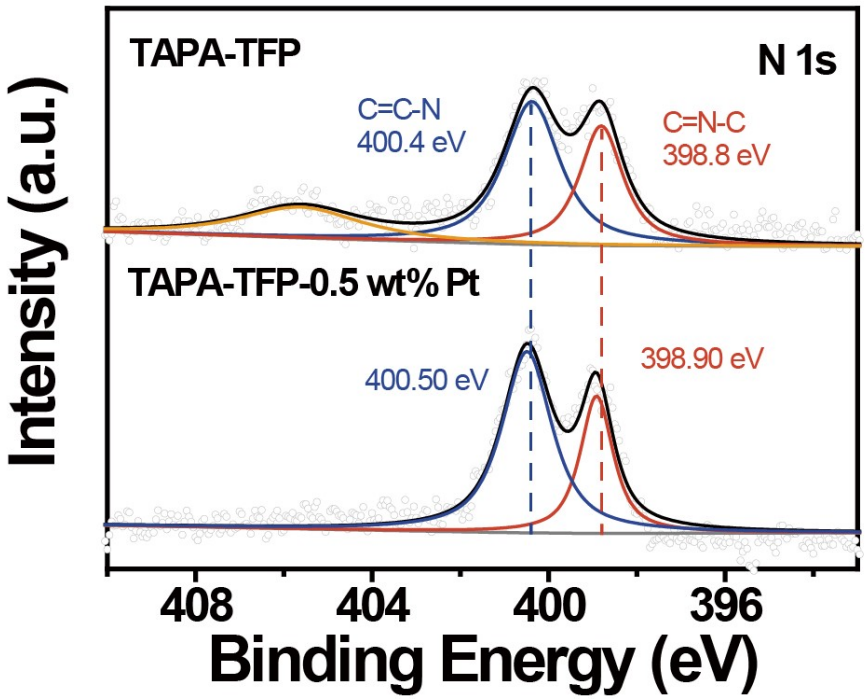

Figure S41. The high-resolution N 1s XPS spectra of pristine TAPA-TFP and COF with Pt additive amount of 0.5 wt%.

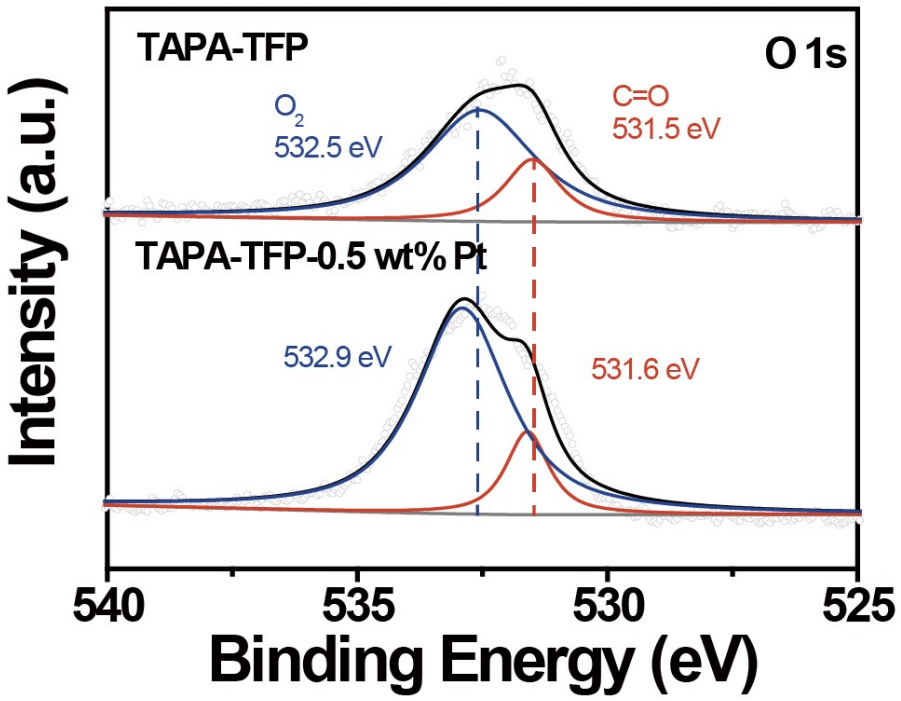

Figure S42. The high-resolution O 1s XPS spectra of pristine TAPA-TFP and COF with Pt additive amount of 0.5 wt%.

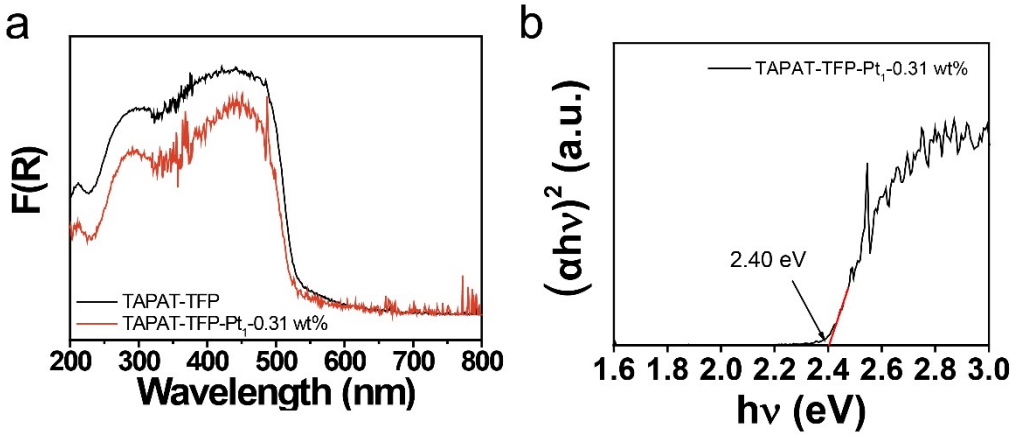

Figure S43. UV-Vis DRS spectrum and tauc plot of TAPAT-TFP-Pt_1.

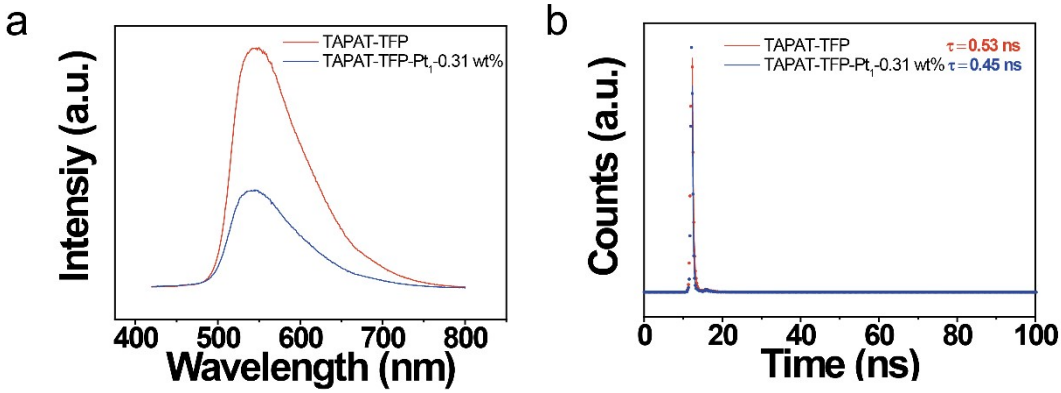

Figure S44. FL and FL decay profiles of TAPAT-TFP-Pt_1 and TAPAT-TFP.

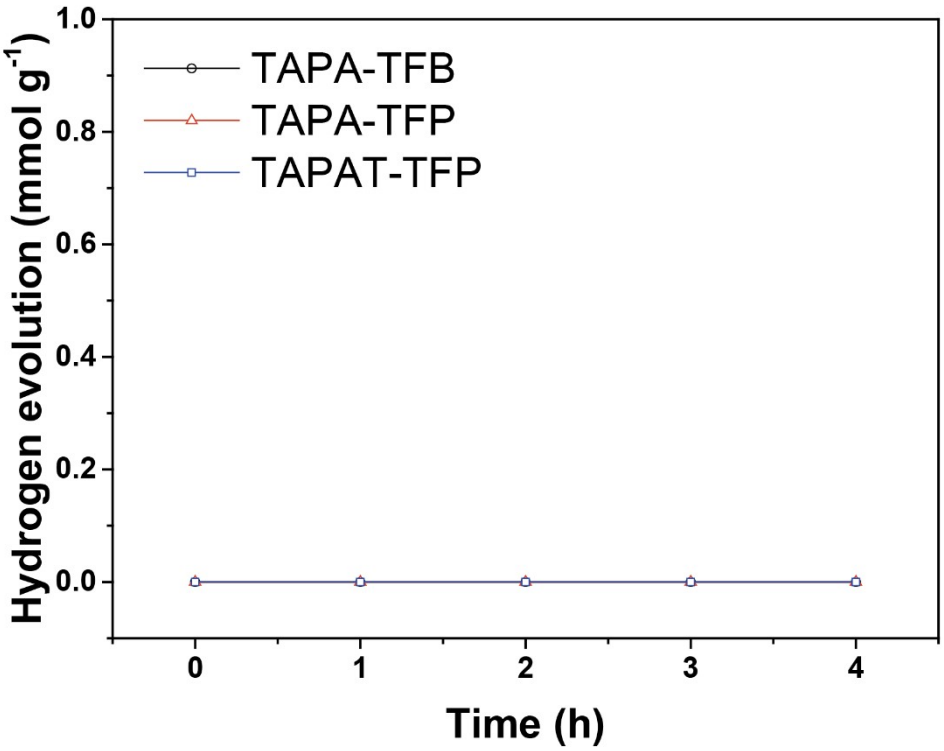

Figure S45 Photocatalytic HER performances of pristine COFs.

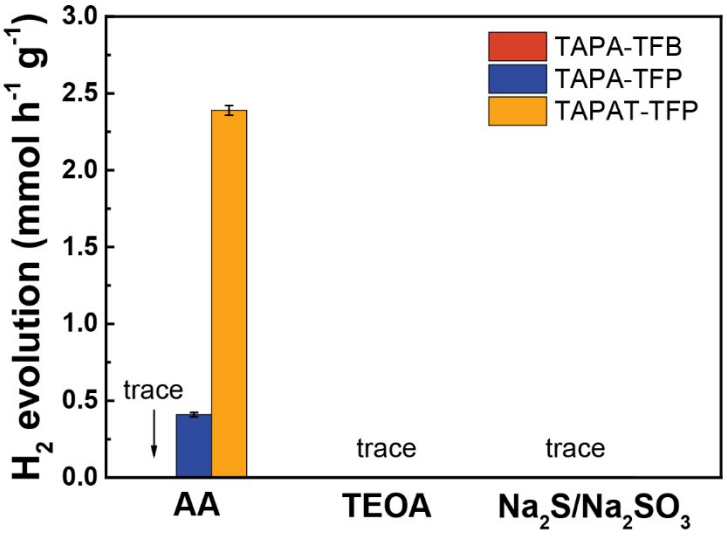

Figure S46 HER performances using various sacrificial agents (TEOA: triethanolamine).

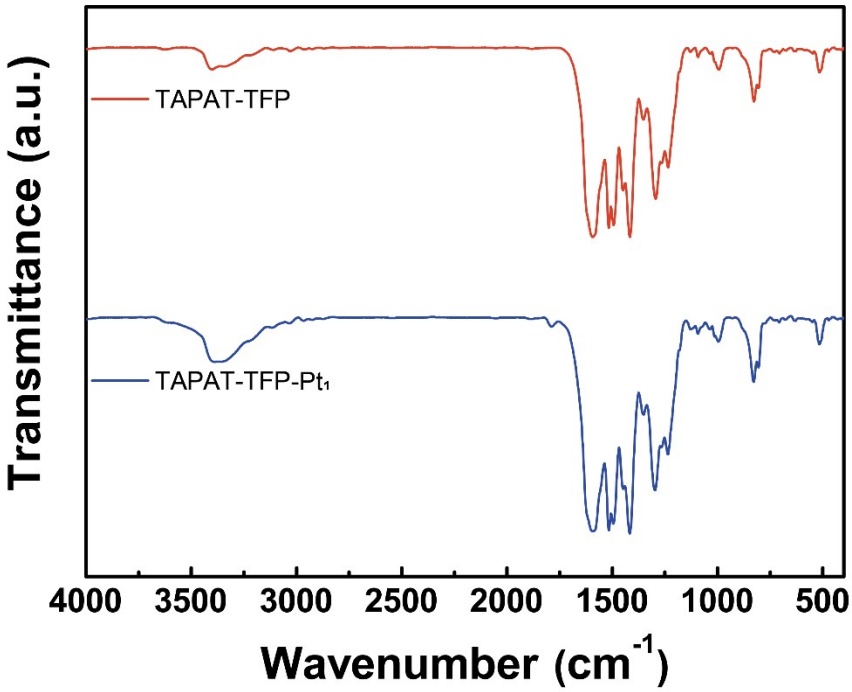

Figure S47. FT-IR patterns of recycled TAPAT-TFP-Pt_1 after photocatalysis.

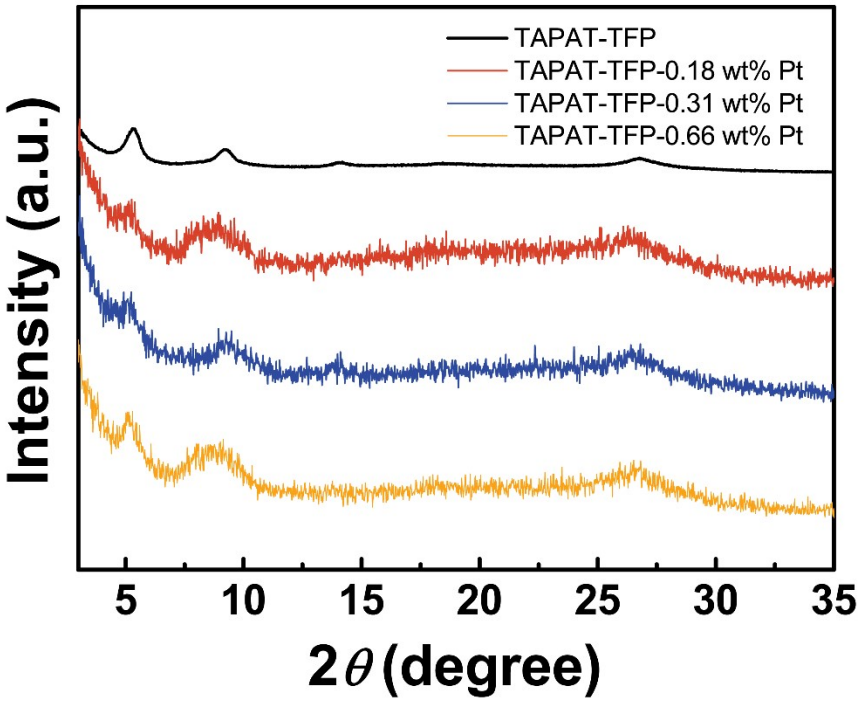

Figure S48. PXRD patterns of recycled TAPAT-TFP-x wt% (additive amount) Pt after photocatalysis.

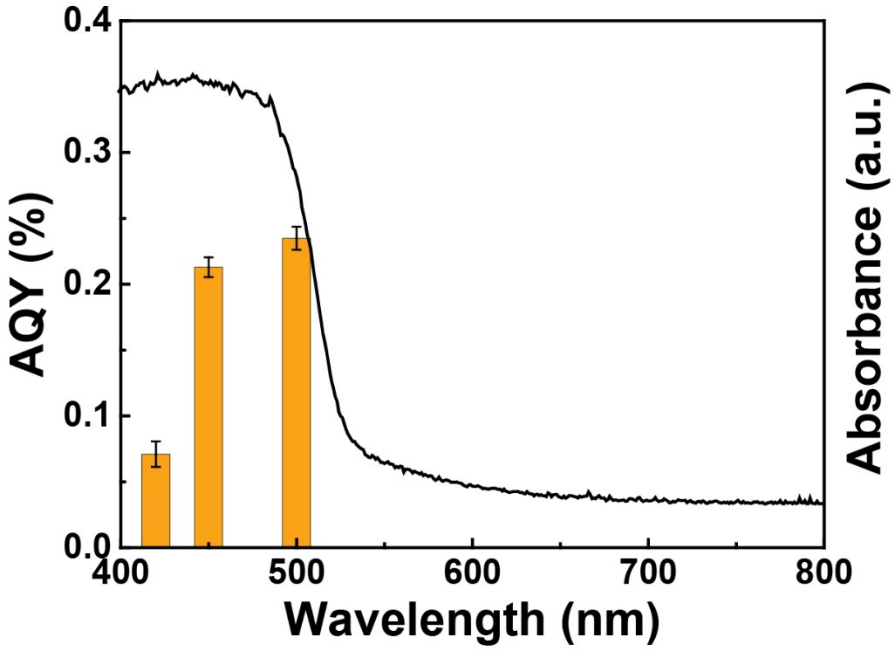

Figure S49. AQY measured at 420 nm, 450 nm, 500 nm and 600 nm using TAPAT-TFP-Pt_1.

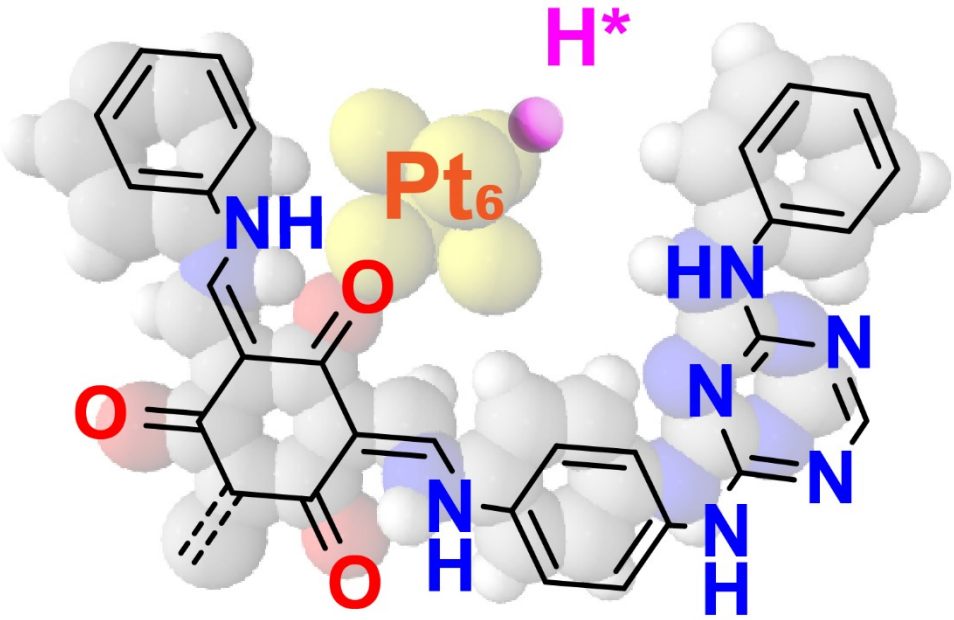

Figure S50. Optimized geometric structures of hydrogen adsorbing on TAPAT-TFP-Pt-NP.

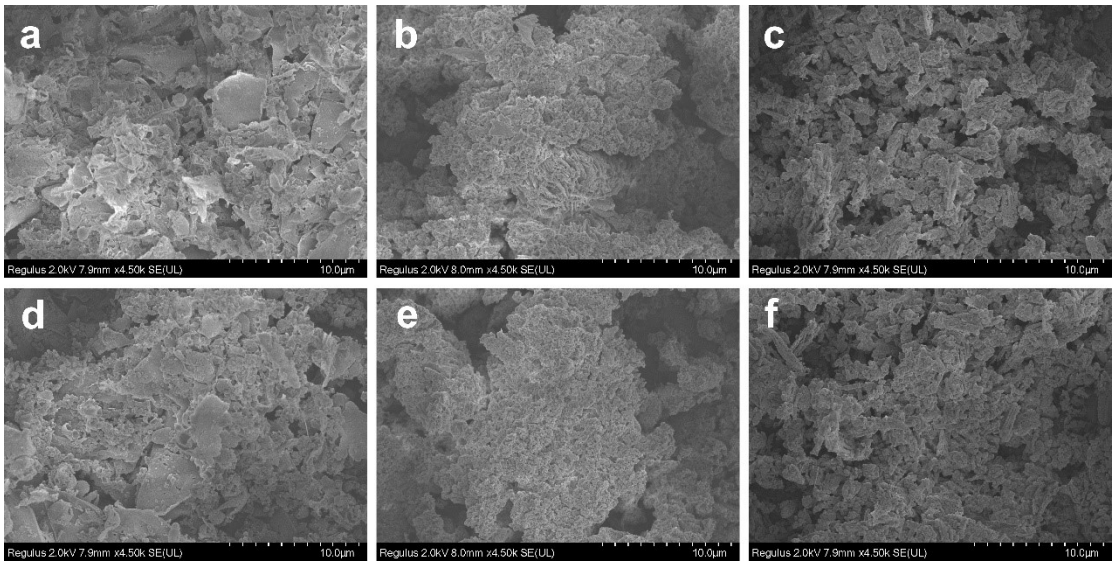

Figure S51. SEM images of recycled TAPA-TFB (a, d), TAPA-TFP (b, e) and TAPAT-TFP (c, f) with the Pt addictive amount of 0.5 wt%.

Table S1 Specific values for $PtCl_6^{2-}$ adsorption on different COF sites.

	site 1	**site 2**	**site 3**
TAPA-TFB	-0.13 eV	-0.31 eV	-0.37 eV
TAPA-TFP	-0.27 eV	-0.40 eV	-0.70 eV
TAPAT-TFP	-0.38 eV	-0.39 eV	-0.72 eV

Table S2 Pt 4f XPS spectra fitting peaks of COFs, as illustrated in Figure 4j-l.

Sample	**peak 1**	**peak 2**	**peak 3**	**peak 4**
TAPA-TFB-Pt	71.6 eV	73.0 eV	75.1 eV	76.5 eV
TAPA-TFP-Pt	71.9 eV	73.3 eV	75.5 eV	76.7 eV
TAPAT-TFP-Pt_1	72.6 eV	73.4 eV	76.1 eV	76.6 eV

Table S3. The photocatalytic performance comparison of TAPAT-TFP-Pt_1-0.31 wt% with other recently reported COFs.

COFs	**Actual Pt loaded (wt %)**	**TOF (h^{-1})**
This work	**0.31**	150.40
3% Pt_1@TpPa-1[3]	0.72	19.48
TCOF-Pt SA[4]	1.72	5.69
Pt/AT-CTF-1[5]	0.54	20.34
0.5% PtNPs–TpPa-1[6]	0.51	4322.45
CTF-TPA-Film-5[7]	2.8	542.05
TP-BPyN PCOF[8]	1.171	204.51
Py-HMPA[9]	6	123.31
COF-935[10]	0.075	5150.22
PIm-COF2[11]	2.48	58.34
BTT-BPy-PCOF[12]	3.32	92.84
TCDA-COF[13]	0.908	1521.14

Table S4. Structural parameters obtained from the Pt L_3-edge EXAFS fitting.

Sample	Shell	[a]N	[b]R (Å)	[c]σ² (Å²)	[d]ΔE₀ (eV)	R factor
Pt-foil	Pt-Pt	12	2.76	0.00544	9.07	0.015
TAPAT-TFP-Pt_1	Pt-O/C	2	2.03	0.00002	14.65	0.037
	Pt-Cl	2	2.30	0.01153		
	Pt-C	3	2.96	0.00499		

[a]N: coordination numbers, [b]R: bond distance, [c]σ^2: Debye-Waller factors, [d]ΔE_0: the inner potential correction. R factor: goodness of fit. S_0^2 was set to be 0.70 according to the experimental EXAFS fitting of Pt foil by fixing N as the known crystallographic value.

Table S5 Unit cell parameters and fractional atomic coordinates for TAPA-TFB-AA.

Space group name	P-6
International table number	174
Crystal system	hexagonal
Lengths	a = b = 18.1590 Å, c = 3.4970 Å
Angles	α = β = 90°, γ = 120°

Atom	x/a	y/b	z/c
H	1.37168	0.88052	0.5
C1	0.15464	0.56364	0.5
N2	0.10738	0.59749	0.5
C3	-0.15691	0.43862	0.5
C4	-0.10235	0.40528	0.5
H5	-0.12561	0.34534	0.5
C6	-0.01667	0.45691	0.5
H7	0.01947	0.43286	0.5
C8	0.01824	0.54298	0.5
C9	-0.03574	0.57862	0.5
H10	-0.01218	0.63874	0.5
C11	-0.12258	0.52527	0.5
H12	-0.1592	0.54868	0.5
C13	0.36742	0.75401	0.5
C14	0.28036	0.70135	0.5
H15	0.23669	0.72988	0.5
C16	0.61655	0.36657	0.5
N17	0.70015	0.41959	0.5

Table S6 Unit cell parameters and fractional atomic coordinates for TAPA-TFB-AB.

Space group name	P-3
International table number	147
Crystal system	trigonal
Lengths	a = b = 18.1590 Å, c = 7.0000 Å
Angles	α = β = 90°, γ = 120°

Atom	x/a	y/b	z/c
H1	1.78991	1.95627	0.24583
C2	1.81847	1.91624	0.27743
N3	1.77312	1.83846	0.33328
C4	1.50902	1.73403	0.40644
C5	1.54339	1.68331	0.34894
H6	1.49993	1.61624	0.31793
C7	1.63058	1.71849	0.32755
H8	1.65784	1.68012	0.27827
C9	1.68592	1.80555	0.3636
C10	1.65179	1.85526	0.43255
H11	1.69464	1.92122	0.47467
C12	1.56451	1.82009	0.45033
H13	1.53756	1.85867	0.49963
N14	1.38695	1.75342	0.41614
C15	1.91069	1.95802	0.25874
C16	1.41612	1.69824	0.41543
C17	1.04687	1.08889	0.74316
H18	1.08449	1.15829	0.73811

Table S7 Unit cell parameters and fractional atomic coordinates for TAPA-TFP-AA.

Space group name	P-6
International table number	174
Crystal system	hexagonal
Lengths	a = b = 18.1590 Å, c = 3.4970 Å
Angles	α = β = 90°, γ = 120°

Atom	x/a	y/b	z/c
O1	1.5169	0.77163	0.5
H2	1.52375	0.85571	0.5
H3	1.508	1.6364	0.5
C4	0.15464	0.56364	3.5
N5	0.10738	0.59749	3.5
C6	-0.15691	0.43862	3.5
C7	-0.10235	0.40528	3.5
H8	-0.12561	0.34534	3.5
C9	-0.01667	0.45691	3.5
H10	0.01947	0.43286	3.5
C11	0.01824	0.54298	3.5
C12	-0.03574	0.57862	3.5
H13	-0.01218	0.63874	3.5
C14	-0.12258	0.52527	3.5
H15	-0.1592	0.54868	3.5
C16	0.36742	0.75401	0.5
C17	0.28036	0.70135	0.5
C18	0.61655	0.36657	0.5
N19	0.70015	0.41959	0.5

Table S8 Unit cell parameters and fractional atomic coordinates for TAPA-TFP-AB.

Space group name	P-3
International table number	147
Crystal system	trigonal
Lengths	a = b = 18.1590 Å, c = 7.0000 Å
Angles	α = β = 90°, γ = 120°

Atom	x/a	y/b	z/c
H1	1.78603	1.91432	0.13308
O2	2.1752	2.10084	0.2532
C3	1.8181	1.90042	0.24976
N4	1.77421	1.84536	0.379
C5	1.50896	1.73747	0.3606
C6	1.54535	1.68508	0.36566
H7	1.50324	1.61628	0.36459
C8	1.63299	1.72037	0.37256
H9	1.66228	1.68049	0.37683
C10	1.68525	1.80899	0.36957
C11	1.64938	1.86184	0.3638
H12	1.69137	1.93075	0.36612
C13	1.56173	1.82611	0.36001
H14	1.53257	1.86603	0.35605
N15	1.38522	1.75355	0.35772
C16	2.08877	2.0507	0.25187
C17	1.91093	1.94902	0.25099
C18	1.41613	1.69996	0.35783

Table S9 Unit cell parameters and fractional atomic coordinates for TAPAT-TFP-AA.

Space group name	P-3
International table number	143
Crystal system	trigonal
Lengths	a = b = 20.2649 Å, c = 3.5350 Å
Angles	α = β = 90°, γ = 120°

Atom	x/a	y/b	z/c
C1	0.06192	0.07061	-0.87246
N2	-0.00987	0.06553	-0.87278
N3	0.12396	0.1468	-0.85286
C4	0.20539	0.17651	-0.85367
C5	0.24105	0.13688	-1.03284
C6	0.32276	0.17222	-1.04118
C7	0.37222	0.24726	-0.86162
C8	0.3347	0.28611	-0.68506
C9	0.25338	0.25193	-0.68565
N10	0.45228	0.286	-0.85541
C11	0.49397	0.25079	-0.9159
C12	0.57587	0.29117	-0.98478
C13	0.62059	0.37744	-1.01272
H14	0.1123	0.19729	-0.83209
H15	0.20232	0.07559	-1.17095
H16	0.35209	0.14109	-1.19498
H17	0.37221	0.34683	-0.53926
H18	0.22478	0.28532	-0.54806
H19	0.46337	0.18292	-0.91426
O	0.58735	0.41744	-0.01486

H	0.48623	0.3511	-0.79677

Table S10 Unit cell parameters and fractional atomic coordinates for TAPAT-TFP-AB.

Space group name	P-3
International table number	143
Crystal system	trigonal
Lengths	a = b = 19.3563 Å, c = 6.7465 Å
Angles	α = β = 90°, γ = 120°

Atom	x/a	y/b	z/c
C1	-0.59982	-0.26454	-0.96065
N2	-0.66894	-0.26287	-0.96174
N3	-0.53216	-0.19074	-0.96261
C4	-0.45383	-0.1723	-0.92578
C5	-0.43476	-0.22818	-0.85179
C6	-0.35621	-0.20566	-0.81544
C7	-0.29538	-0.12716	-0.84801
C8	-0.31455	-0.07144	-0.92336
C9	-0.39308	-0.09386	-0.96086
N10	-0.21666	-0.10988	-0.81494
H11	-0.40835	-0.04804	-1.02079
H12	-0.34017	-0.25127	-0.75809
H13	-0.48408	-0.29202	-0.82182
H14	-0.26529	-0.0076	-0.95368
H15	-0.53634	-0.13684	-0.99661
C16	-0.16237	-0.03728	-0.77488
C17	-0.07946	-0.01814	-0.75751
C18	-0.06097	-0.0792	-0.75644

H19	-0.1796	0.0106	-0.75373
H20	-0.1094	-0.1412	-0.76119
H	-0.2017	-0.15819	-0.82333

Reference:

1. B. Ravel and M. Newville, *J. Synchrotron Radiat.*, 2005, **12**, 537-541.
2. X. Xu, H. Xu and D. Cheng, *Nanoscale*, 2019, **11**, 20228-20237.
3. P. Dong, Y. Wang, A. Zhang, T. Cheng, X. Xi and J. Zhang, *ACS Catal.*, 2021, **11**, 13266-13279.
4. Y. Xia, B. Zhu, L. Li, W. Ho, J. Wu, H. Chen and J. Yu, *Small*, 2023, **19**, e2301928.
5. L. L. Zheng, X. Li, D. Wang, Y. Chen, Q. Fu, D. S. Wu, X. Z. Liu and J. P. Zou, *Nanoscale*, 2024, **16**, 6010-6016.
6. Z. Zhao, W. Chen, G. Zhang and Y. Chen, *J. Mater. Chem. A*, 2023, **11**, 26052-26062.
7. Y. Guo, X. Hu, R. Sun, X. Wang and B. Tan, *ChemSusChem*, 2023, **16**, e202300759
8. X. Gao, J. Yuan, P. Wei, J. Dong, L. Chang, Z. Huang, H. Zheng, J. Liu, J. Jia, T. Luan, B. Zhou, H. Yu and C. Peng, *ACS Catal.*, 2023, **14**, 533-546.
9. Y. Liu, W.-K. Han, W. Chi, J.-X. Fu, Y. Mao, X. Yan, J.-X. Shao, Y. Jiang and Z.-G. Gu, *Appl. Catal. B Environ.*, 2023, **338**, 123074.
10. K. Wang, Y. Zhong, W. Dong, Y. Xiao, S. Ren and L. Li, *Angew. Chem. Int. Ed.*, 2023, DOI: 10.1002/anie.202304611, e202304611.
11. C.-X. Liu, D.-L. Pan, Y. Seo, S. Park, J.-L. Kan, J. Y. Koo, W. Choi and E. Lee, *ACS Appl. Energy Mater.*, 2023, **6**, 1126-1133.
12. L. Dai, A. Dong, X. Meng, H. Liu, Y. Li, P. Li and B. Wang, *Angew. Chem. Int. Ed.*, 2023, **62**, e202300224.

13. Z. Li, T. Deng, S. Ma, Z. Zhang, G. Wu, J. Wang, Q. Li, H. Xia, S.-W. Yang and X. Liu, *J. Am. Chem. Soc.*, 2023, **145**, 8364−8374.